Dissertationes Forestales 356

Whole-tree Lagrangian optimal stomata model and its application to predicting cambial growth of tree stem

Che Liu

Department of Forest Sciences
Faculty of Agriculture and Forestry
University of Helsinki

Academic dissertation

To be presented, with the permission of the Faculty of Agriculture and Forestry of the University of Helsinki, for public examination in Auditorium B2, Forest Sciences Building (Viikki Campus, Latokartanonkaari 7, Helsinki) on 8th November 2024 at 13:00

Title of dissertation: Whole-tree Lagrangian optimal stomata model and its application to predicting cambial growth of tree stem
Author: Che Liu

Dissertationes Forestales 356
https://doi.org/10.14214/df.356

Thesis supervisors:
Professor emerita Annikki Mäkelä
Department of Forest Sciences, University of Helsinki, Finland
Professor Teemu Hölttä
Department of Forest Sciences, University of Helsinki, Finland

Preliminary examiners:
Distinguished Professor Belinda Medlyn
Hawkesbury Institute for the Environment, Western Sydney University, Australia
Senior Researcher Liisa Kulmala
Finnish Meteorological Institute, Finland

Opponent:
Professor Andrew Friend
Department of Geography, University of Cambridge, UK

ISSN 1795-7389 (online)
ISBN 978-951-651-802-5 (pdf)

Publishers:
Finnish Society of Forest Science
Faculty of Agriculture and Forestry, University of Helsinki
School of Forest Sciences, University of Eastern Finland

Editorial office:
Finnish Society of Forest Science
Viikinkaari 6, 00790 Helsinki, Finland
https://www.dissertationesforestales.fi

Liu, Ch. 2024. Whole-tree Lagrangian optimal stomata model and its application to predicting cambial growth of tree stem. Dissertationes Forestales 356. 62 pp. https://doi.org/10.14214/df.356

ABSTRACT

Stomata are a pivotal nexus between tree physiology and the environment, and thus modelling stomatal behaviour is critical for understanding tree growth and functioning. One of such models that have been widely tested is based on Lagrangian optimality analysis of gas exchange. The objectives of the present study were expanding the optimal stomata model to the whole-tree scale and coupling it with a model of cambial growth. The coupled model connects stomatal behaviour with non-stomatal limitation on photosynthesis, waterlogging effects, and the enzymatic activities and phenology of cambial growth. It requires commonplace inputs of meteorology, photosynthetic photon flux density (PPFD) and soil water conditions and can output transpiration, assimilation and cambial growth rates simultaneously at 30-minute resolution. The model was parameterized using Bayesian statistics and tested against observations on *Pinus sylvestris* and *Picea abies* from boreal forest sites in Finland of peatland and mineral soils. The model performance on simulating transpiration rate and stem radial dimension was good. Statistical analyses of model parameters showed that young/short trees almost always had higher stomatal conductance than old/tall trees under typical vapour pressure deficit (VPD) and PPFD. Also, maximum soil-to-root hydraulic conductance and minimum marginal water use efficiency (MWUE) of the trees were positively correlated with their leaf-to-sapwood area ratio. The modelled cambial growth duration was positively correlated with leaf-specific photosynthetic production (P) of the growing season at the moister peatland but not at the dryer mineral-soil site, and otherwise phenological traits of cambial growth were not significantly correlated with P at either site, suggesting P is not sufficient for determining the growth phenology of boreal trees. The model provides an easy-to-use tool for coupled tree eco-physiological and growth simulation and insights into larger-scale sink-driven vegetation modelling.

Keywords: Bayesian inference, cambial growth, mechanistic modelling, stomatal optimality, tree hydraulics

Philosophari enim est,
effectus iam cogniti certam et
manifestam et veram causam
investigare, et ostendere
quomodo illius causa est.

Alberti Magni
De Vegetabilibus et Plantis

To philosophize is so,
to investigate the certain,
manifest and true cause of
a known effect, and to explain
how the cause is being.

Albertus Magnus
De Vegetabilibus et Plantis

LIST OF ORIGINAL ARTICLES

The dissertation is based on the following research articles, which are referred to by their Roman numerals (boldface) in the main text.

I Liu Ch, Hölttä T, Tian X-L, Berninger F, Mäkelä A. (2020). Weaker light response, lower stomatal conductance and structural changes in old boreal conifers implied by a Bayesian hierarchical model. *Frontiers in Plant Science* 11: article id 579319. DOI: 10.3389/fpls.2020.579319

II Liu Ch, Wang Q, Mäkelä A, Hökkä H, Peltoniemi M, Hölttä T. (2022). A model bridging waterlogging, stomatal behaviour and water use in trees in drained peatland. *Tree Physiology* 42: 1736-1749. DOI: 10.1093/treephys/tpac037

III Liu Ch, Peltoniemi M, Alekseychik P, Mäkelä A, Hölttä T. (2024). A coupled model of hydraulic eco-physiology and cambial growth at high temporal resolution – accounting for biophysical limitations and phenology improves stem diameter prediction at high temporal resolution. *Plant, Cell & Environment*. DOI: 10.1111/pce.15239.

Author's contribution

I Ch. Liu was the main author, co-designed and programmed for the model, and executed the fieldwork for data collection.

II Ch. Liu was the main author, co-designed and programmed for the model, and participated in data processing.

III Ch. Liu was the main author, co-designed and programmed for the model, and participated in data processing.

SYMBOLS

The following list comprises the Latin and Greek letters used in the core model, excluding conventional mathematical notations (e.g. d for differentiation) or SI units (e.g. m for the metre). The modified symbols exclude 1) boldface, denoting a matrix or a vector, 2) the dot notation, denoting derivative with respect to time (and only to time; e.g. $\dot{E} \stackrel{\text{def}}{=} \mathrm{d}E(t)/\mathrm{d}t$), and 3) parameter with hat (circumflex; e.g. $\hat{\iota}$), denoting its maximum a posteriori (MAP) estimate. Constant values and/or typical units, if applicable, are displayed in parentheses at the end of definitions. The uses of symbols may differ from those in the attached original articles for the consistency of the main text.

A Assimilation rate (mol m^{-2} s^{-1})

b Coefficient in the water retention curve of growing media (soil and peat).

C (Linear) Hydraulic capacitance (mm MPa^{-1})
Subscript: C_b, C of the bark.

$\mathcal{C}$ CO_2 concentration (mol m^{-3})
Subscripts: $\mathcal{C}_a$, atmospheric $\mathcal{C}$; $\mathcal{C}_i$, intercellular $\mathcal{C}$.

c Slope parameter between the initial slope (ι) of photosynthetic photon flux density (I) response curve and acclimation of foliage to temperature (S) (m^3 (mol C°)$^{-1}$)

D Vapour pressure deficit (VPD) (mol m^{-3})

d Water table depth (WTD) (cm)
Superscript: d^*, optimal d corresponding to the optimal soil water content (θ^*).

d_c Radial diameter of a cambial cell
Modifier: $\bar{d}_c$, average d_c (*Picea abies*, 0.035 mm; *Pinus sylvestris*, 0.0325 mm)

E Transpiration rate (mol m^{-2} s^{-1})
Superscripts: $E^{(M)}$, modelled E.

$\mathcal{E}$ Modulus of elasticity (of the wood section of interest) (MPa)
Subscript: $\mathcal{E}_b$, $\mathcal{E}$ of the bark.

g_c Cambial cell relative expansion rate

g_σ (Optimal) Stomatal conductance (m s^{-1})
Modifiers: g_σ^*, optimal stomatal conductance, used in preliminary mathematical demonstration; g_0, minimum conductance (*Picea abies*, 4.5525×10^{-5} m s^{-1}; *Pinus sylvestris*, 7.5×10^{-5} m s^{-1}).

ΔH Enthalpy difference (J mol^{-1})
Subscripts: ΔH_a, enthalpy of activation of enzymatic system, i.e. ΔH between enzymatic system's transition state and reactant; ΔH_d, ΔH between enzymatic system's catalytically active and inactive states.

h (Tree) height (m)
Subscript: h_{rb}, height between average depth of active fine roots and breast height (1.5 m); h_{rl}, root-to-leaf height.

I Photosynthetic photon flux density (PPFD) (mol m^{-2} s^{-1})

J Sap flow (substance) density (mol m^{-2} s^{-1})
Superscript: $J^{(O)}$, observed J.

K Hydraulic conductivity (mol m^{-1} s^{-1} Pa^{-1})
Subscript: K_{sat}, saturated soil K.

k Hydraulic conductance (mol m^{-2} s^{-1} Pa^{-1})
Subscripts: k_0, base-case (soil-to-leaf) k; k_{bc}, k between the bark and the cambium; k_{DS}, k_{sr} in deep mineral soil (C horizon) (8.8×10^{-10} mol m^{-2} s^{-1} Pa^{-1}); k_{rb}, root-to-breast height k; k_{rl}, root-to-leaf k; k_{sb}, soil-to-breast height k; k_{sl}, soil-to-leaf k; k_{sr}, soil-to-root k.

l Dimension (mm).
Modifiers: l_0, initial value of l_{BH}; l_{b0}, initial bark thickness; l_{BH}, diameter or radius of tree trunk at breast height; l_{ela}, l_{BH} component related to elasticity; l_{gro}, l_{BH} component due to irreversible growth.

$\mathcal{M}$ Michaelis constant of intercellular CO_2 kinetics

m Displacement parameter of the Gompertz function

N Number related to the cambial cell
Subscripts: N_c, N of active cambial cells; N_c^{max}, maximum N_c; N_D, N of times of cambial cell volume (V) doubling.

n Number of elements in an error matrix ($\boldsymbol{\varepsilon}$)

$\wp$ Rainfall intensity (mm s^{-1}).

Q_{10} Relative increase of respiration rate (R) per 10 °C

q_b Water storage of the bark (mm)

R Respiration rate (mol m^{-2} s^{-1})
Subscript: R_0, R at 0 °C.

S Photosynthetic acclimation of foliage to temperature (T_l) above reference level (°C)
Subscript: S_0, reference level for S.

ΔS_d Entropy difference between enzymatic system's catalytically active and inactive states (J mol^{-1} K^{-1}).

T (Air) Temperature (°C)
Subscripts: T_0, threshold T of cambial cell growth; T_l, leaf temperature.

$\mathcal{T}$ Time unity

t Time

u Water flow (volume) density (mm s^{-1})
Modifiers: u_{bin}, u influx of the bark due to precipitation; u_{bin}^{max}, maximum u_{bin} (2×10^{-5} mm s^{-1}); u_{bc}, u efflux of the bark to the cambium.

V Cell volume

$\mathcal{V}_c^{max}$ Maximum carboxylation capacity without non-stomatal limitation (mol m^{-2} s^{-1})

$\mathcal{W}$ Water vapour concentration (mol m^{-3})
Subscripts: $\mathcal{W}_a$, ambient (atmospheric) $\mathcal{W}$; $\mathcal{W}_i$, intercellular $\mathcal{W}$.

z Parameter in the log-log linear correlation between marginal carbon gain per water cost (λ) and soil-to-leaf conductance relative to the base-case value (k_{sl}/k_0)
Subscripts: z_0, intercept; z_1, slope.

α Scaling coefficient in cell wall extensibility (5.3544×10^{12} K^{-1})

β Slope parameter between the hydraulic time lag (χ) and tree height (minute per m)

Γ^* CO_2 compensation point in photosynthesis (mol m^{-3})

γ Saturation level of PPFD response curve (m s^{-1})

ε Error term
Subscripts: ε_D, ε of the tree stem radial dimension (SRD) model. ε_L, ε of the whole-tree Lagrangian optimal stomata model (LOSM).

η Parameter in soil-to-root conductance (k_{sr}) as a decreasing function of soil water content (θ)
Subscripts: η_m, multiplier; η_p, power.

Θ Assimilation deficit (mol m^{-2} s^{-1})

θ Soil water content (m^3 m^{-3})
Modifiers: θ_{res}, residual θ; θ_{sat}, saturated θ; θ^*, optimal θ regarding soil-to-root conductance.

ι Initial slope of PPFD response curve (m^3 mol^{-1})

λ The Lagrange multiplier, or the marginal carbon gain per water cost (mol mol^{-1})
Subscript: $\lambda_{(CF)}$, the original Lagrange multiplier by Cowan and Farquhar (1977).

ξ Parameter in soil-to-root conductance (k_{sr}) as an increasing function of soil water content (θ)
Subscripts: ξ_m, multiplier; ξ_p, power.

ρ Ratio related to tree structure
Subscripts: ρ_{lw}, ρ of all-sided leaf to sapwood areas (m^2 m^{-2}); ρ_{rl}, ρ of root length to all-sided leaf area (m m^{-2}); ρ_{rr}, ρ of rhizosphere to mean hydraulically active root diameters (m m^{-1}).

τ Time constant
Subscripts: τ_c, τ of the cambial cell expansion rate ($\mathcal{g}$) (hour); τ_S, τ of the photosynthetic acclimation of foliage to temperature (S) (day).

φ Impact coefficient of low leaf water potential (ψ_l) on assimilation rate (A)

ϕ Cell wall extensibility
Subscript: ϕ_{max}, maximum ϕ.

χ Time lag between transpiration (E) and sap flow density at tree base (J) (minute)

ψ (Water) Potential (Pa or MPa)
Modifiers: ψ_{A0}, critical leaf ψ regarding photosynthesis (-2 MPa); $\Delta\psi_{bc}$, turgor (hydrostatic potential) difference between bark and cambium; ψ_e, soil ψ of air entry; $\psi_{\mathcal{g}0}$, threshold ψ of cambial cell growth; $\Delta\psi_g$, ψ difference due to gravity; ψ_l, leaf ψ; ψ_p, turgor; ψ_p^{cam}, ψ_p of cambium (at breast height); ψ_s, soil ψ; ψ_{sat}, saturated ψ_s.

CONTENTS

INTRODUCTION

A key primary producer and the predominant terrestrial ecosystem, forests cover 31% (4.06×10^7 km^2) of the total land area of Earth and hold 6.62×10^{11} tonnes of carbon, of which 44% is in living biomass (FAO 2020). Their gross primary production (GPP) reaches 123 ± 8 Pg carbon per year (75% of the total GPP of all terrestrial ecosystems), and 40% of which is correlated with precipitation (Beer et al. 2010). Thus, forests play a pivotal role in global carbon balance and interact with hydraulic environment significantly. Not only do trees' physiological activities (e.g. photosynthesis) rely on atmospheric and environmental water conditions, but they also regulate climate and thus mitigate natural hazards e.g. drought and flood (Bradshaw et al. 2007; Wright et al. 2017). As the risks of drought or flood are increasing under the changing climates (IPCC 2023), our understanding and prediction of trees' functioning and growth in relation to environmental water conditions are valuable for corresponding mitigation measures. In terms of these purposes, mathematical modelling is an indispensable tool for describing, understanding, theorizing and predicting related phenomena and processes.

Modelling stomatal behaviour

Stomata are the nexus between trees and the environment regarding hydraulics and photosynthesis. They control the gas (carbon dioxide [CO_2] and water vapour) exchange between leaves and the atmosphere, which generates the driving pressure (water potential) of transpiration and water uptake from the soil. Modelling stomatal behaviour starts with physical analyses of gas exchange at the aperture. In one of the first systematic modelling works on stomatal conductance and transpiration rate, Jarvis (1976) applied the Penman-Monteith equation to the microenvironment at stomatal aperture and quantified the water potential due to transpiration. Thereafter, the effects of environmental factors are included to connect the formulated water potential and transpiration rate with local meteorology. The factors, namely photosynthetic photon flux density (PPFD, I), leaf temperature (T_l), water vapour pressure deficit (VPD, D), leaf water potential (ψ_l) and atmospheric CO_2 concentration ($\mathcal{C}_a$), are directly linked with stomatal conductance (g_σ) algebraically without expressing intermediate mechanisms. The interactions among the effects are omitted at synergizing. That is to say

$$g_\sigma(I, T_l, D, \psi_l, \mathcal{C}_a) = g_\sigma(I) g_\sigma(T_l) g_\sigma(D) g_\sigma(\psi_l) g_\sigma(\mathcal{C}_a) \quad (1)$$

This simplified equation facilitates model calibration using data of one or several specific factors and partitioning their effects. Employing analogies to electrical network as well as statistical tools, Jarvis and McNaughton (1986) later developed this model to whole-leaf (mechanistically) and larger (e.g. whole-canopy, statistically) spatial scales. This series of models has been incorporated into widely used ecosystem- or global-scale ecological models (e.g. Sellers et al. 1986; Collatz et al. 1991; Cramer et al. 2001). Nevertheless, their applicability is limited by the absence of 1) interactions among environmental factors and 2) an explicit expression of photosynthetic processes. To improve in these aspects, a semi-process-based module on photosynthesis was added in for formulating stomatal functionality more mechanistically and holistically (Ball et al. 1987; Leuning

1995). The module is based on Fick's law of diffusion, and thus assimilation rate (A) is expressed as

$$A = g_\sigma(\mathcal{C}_\mathrm{a} - \mathcal{C}_\mathrm{i}) \tag{2}$$

where $\mathcal{C}_\mathrm{i}$ is intercellular CO_2 concentration, and for transpiration rate (E)

$$E = 1.6 g_\sigma(\mathcal{W}_\mathrm{i} - \mathcal{W}_\mathrm{a}) \equiv 1.6 g_\sigma D \tag{3}$$

where $\mathcal{W}_\mathrm{i}$ and $\mathcal{W}_\mathrm{a}$ are intercellular and ambient water vapour concentrations, respectively, between which the difference is essentially VPD (D), and 1.6 is the dimensionless ratio of H_2O to CO_2 diffusion rates. Despite the empirical simplification based on experiments to derive the expression of g_σ in similar forms of Eq. 1, the model's physical basis enables mechanistic interpretations of guard cell functioning and further development of accounting for intercellular processes involving CO_2 dynamics (Dewar 1995). Meanwhile, attempts of integrating models of stomatal control and root water flux were made by linking them via the effect of abscisic acid (ABA) concentration on osmotic water potential (e.g. Tardieu and Davies 1993). Tardieu and Davies (1993) have also improved the performance of earlier models (Ball et al. 1987; Leuning 1995) on drought-stressed plants as these previous models' empirical simplification fails to simulate the hydraulics under extremely dry conditions. Dewar (2002) combined these models within one mechanistic framework featuring guard cell osmotic balance, soil-to-root conductance as a function of soil water potential and whole-plant hydraulic network analysis. So far, this framework has been extended to cover hydraulic eco-physiology of trees across multiple scales and tested against various observations. Thus, it provides a paradigm for the present study on expanding the scope and applicability of another stomata model that features the optimality theory.

The stomatal optimality model starts with Cowan and Farquhar's (1977) definition that the optimal stomatal control realizes minimal summed water loss and maximal summed carbon gain during a time (e.g. a day). Hence, solving for optimal g_σ becomes an isoperimetric problem (Cowan 1982), i.e. a problem of a functional's extrema with an isoperimetric constraint. With applying Fick's law of diffusion (Eq. 2 and 3) again and the Euler-Lagrange equation, the optimal g_σ can be solved eventually in relation to D, I, $\mathcal{C}_\mathrm{a}$ and T_l (Hari et al. 1986; Hari and Mäkelä 2003; Mäkelä et al. 2004). The solution of steady-state optimal g_σ has been reconciled with the earlier models (Jarvis 1976; Ball et al. 1987; Leuning 1995; Dewar 2002) on the canopy scale with minor mathematical simplification (Medlyn et al. 2011). Later theoretical studies have expanded the reconciled model to whole-tree applications for various objectives on detailed photosynthetic and/or hydraulic mechanisms. Sperry et al. (2017) accounted for xylem hydraulic vulnerability, analysed its impacts on stomatal responses, and concluded that stomata can adjust their aperture along a continuum of possible steady states depending on photosynthetic profit (i.e. $A - E$). Hölttä et al. (2017) incorporated sugar transport into their model and showed how stomatal behaviour and whole-tree vascular structure can be linked through the marginal cost of water in assimilation or, in a mathematical term, the Lagrange multiplier in the Euler-Lagrange equation. Dewar et al. (2018) conducted a rigorous comparison of earlier models' performances with non-stomatal limitations on photosynthesis and demonstrated the earlier formulations indeed converge significantly but also diverge in accuracy under varying C_a, which had not been focal in earlier discussions. Recently, Potkay et al. (2021) launched an inspiring attempt to use coupled optimalities of whole-tree hydraulics and stomatal behaviour (Hari et al. 1986) to explain biomass partitioning, shedding light upon the mechanisms behind carbon allocation in trees. Additionally, similar reconciled

optimization models have also been applied to ecosystem or larger spatial scales using empirical (including probabilistic) tools for studying a range of eco-physiological topics, e.g. soil-organism water balance and impacts of drought on tree stands (Manzoni et al. 2013; Lin et al. 2015; Lu et al. 2020).

Nonetheless, there are yet uncertainties and potentials of the whole-tree expansions of optimal stomata models. Firstly, the models have not been tested against continuously measured data at fine temporal resolution (e.g. ≤ 1 hour). Such a test typically forms an inverse problem in modelling, that is, calibrating the model's parameters using observations of input variables. Thus, it demands a proper selection of parameters that reflect key eco-physiological traits, the use of prior knowledge for parameter estimation, and intensive computation. Once such a test is successful, the whole-tree optimal stomata model can potentially provide inputs for downstream models related to hydraulic processes, e.g. simulating the stem radial dimension (SRD). This is because both causes of SRD dynamics, namely, hydraulic changes and growth, depend on water potential, which is induced by transpiration. Cambial cell splitting must meet hydrostatic (turgor) potential threshold as a prerequisite (Lockhart 1965), and hydrostatic potential is also the direct driver of reversible xylem expansion and contraction induced by transpiration. Therefore, a coupled stomatal and growth model should provide a tool accounting for both hydraulic eco-physiology and growth, which should be an important supplement to the existing growth models that are mostly centralized around carbon gain (Fatichi et al. 2019).

Modelling tree stem radial growth

Tree growth is one of the natural phenomena with longest history of mathematical modelling. Traditional descriptive models of annual growth employ algebraically parsimonious formulae to describe year-to-year changes in biological attributes. For example, the Gompertz model (Gompertz 1825) is based on the generic hypothesis that the growth rate of an entity relative to its current state saturates at an asymptote. This simple but versatile model has earned successful applications to tree or stand growth (Winsor 1932; Thornley and Johnson 1990; Zeide 1993). More recent models are intended to formulate growth-related processes, especially carbon sequestration and allocation. For instance, the carbon-balance analysis of tree growth tracks the influxes, effluxes and allocations of carbon related to the organic system of the tree (Mäkelä and Valentine 2020). It formulates a tree as a set of component biomasses (masses of carbon), usually including foliage, fine roots, and woody tissues, and the growth of each component is a fraction of the tree's net production (i.e. gross photosynthetic production minus respiration) subtracting the corresponding sector's litter (McMurtrie and Wolf 1983; Mäkelä 1997). The allocation of photosynthates to the components is subject to environmental control (e.g. fine roots' growth affected by soil water content) and interacts with (affects and receives feedback from) tree structure. Hence, carbon sequestration and allocation are the centre of such models, and environmental control mainly functions via these carbon fluxes.

Carbon-balance growth models have been substantially expanded and performed well with a range of ecological modules, e.g. the competition for light (e.g. Valentine et al. 2000; Duursma and Mäkelä 2007; Härkönen et al. 2010), symbiosis with mycorrhizae (Mäkelä et al. 2022), and continental-scale carbon dynamics (e.g. Mäkelä et al. 2008; Peltoniemi et al. 2015; Tian et al. 2020). However, the central role of carbon gain in modelling growth has been questioned by experimental observations suggesting that tree growth is not carbon-limited (Millard et al. 2007). Thus, the direct

environmental control of cambial/meristematic activities ('sink pathway') has been suggested to act a more significant role in growth and vegetation models (Körner 2015; Fatichi et al. 2019; Friend et al. 2019). Such direct environmental effects on growth-related sink activities become particularly influential when the studied temporal scale is finer than annual (e.g. daily or even hourly). This issue has been addressed in recent models. For instance, Schiestl-Aalto et al. (2015) incorporated the hydraulic requirement for cambial cell expansion into their daily-scale carbon-balance analysis, which also features a more detailed framework of non-structural carbon (NSC) dynamics in the forms of sucrose and starch. Similar in methodology, Hayat et al. (2017) also began with carbon-balance analysis, modified it to express sink limitation using parameters, and presented a framework that reflects tree-age-related shift from source- to sink-limited growth. The models specifically focussed on cambial growth may feature a yet smaller role of carbon source. Hölttä et al. (2010) centred their model around the transport of water and photosynthates and their interaction on water potential regulation, and it provides a successful sink-orientated method including more detailed physiological depiction. Using similar analyses, Chan et al. (2016) modelled both growth and hydraulic fluctuations, focussing also on the environmental effects direct on sink activities while assuming NSC always sufficient for cambial growth. The broad application of the linear displacement transducer or point dendrometer (Deslauriers et al. 2007; Mencuccini et al. 2013) has facilitated testing the models at high temporal resolution ($\leq$ 1 day) while, however, also generated uncertainties.

A foremost challenge in dendrometer application is related to disaggregating the observed SRD to reversible hydraulic changes and irreversible growth. A simple method is to either define the fraction of growth or simulate hydraulic fraction firstly and then take the other as the remainder. Zweifel et al. (2016) have suggested that water potential requirement for cell division and elongation can hardly be fulfilled during the daytime, and thus have defined growth simply as the increment between each two temporal maxima of SRD in the chrono-sequence, assuming zero growth in between. This method has earned wide applications (e.g. Schäfer et al. 2019; Eitel et al. 2020; Güney et al. 2020) for its easy operation, but it may result in dubious growth detection during the winter (Zweifel et al. 2020). Also, the method causes information loss on the temporal scales finer than a day. Alternatively, hydraulic expansion and contraction may be modelled first and subtracted from dendrometer records, and growth is defined as the consequent difference (Chan et al. 2016; Mencuccini et al. 2017). Such modelling methods present mechanistic description of hydraulic processes at the original temporal resolution of data and can capture the dynamics well. However, similar to the challenge in parameterizing whole-tree expansions of stomatal models, difficulty in calibrating SRD models is also considerable, which has limited the application of the few models that simulate hydraulic and growth dynamics simultaneously (e.g. Steppe et al. 2006).

Following these earlier models, the present study was aimed at modelling SRD caused by hydraulic dynamics and growth at high temporal resolution simultaneously and with easy parameterization. The simultaneous simulation should be realized by coupling a whole-tree expansion of optimal stomata model and a growth model focussed on sink activities through water potential, as depicted in the previous section. A model describing the enthalpy and entropies of enzymatic activation was chosen as the basis for its rigorous analysis and fewer inputs and parameters. This model was revived by Parent et al. (2010) from Johnson et al. (1942) biochemical analyses, and Parent and Tardieu (2012) and Cabon et al. (2020) later tested it on temperate crops and coniferous trees. However, it yet needed to be tested on boreal forests, whose low production (Cramer et al. 1999) questions the validity of assuming carbon source always sufficient throughout a growing season. Moreover, the model expresses only the instantaneous (cf. seasonal-scale) effects of the environment on cambial activities, which is challenged by the strong phenology in

the boreal zone (Kramer et al. 2000; Delpierre et al. 2016a). Carbon source and cambial growth phenology of boreal trees may correlate with each other in the following aspects. In early spring, low carbon gain may result in delayed growth onset, as boreal conifers 'prioritize' carbon storage over growth under constrained carbon gain (Huang et al. 2021). Also, if carbon gain fails to fulfil the trees' demand of soluble sugars that help defend against frost damages in early spring (Hartmann and Trumbore 2016; D'Andrea et al. 2021), the trees will experience a slower physiological recovery from wintry conditions and thus a later growth onset as well (Linkosalo et al. 2006; Begum et al. 2013). The duration of growth relates to carbon gain in the spring with respect to the accumulation of non-structural carbohydrates (NSC), whose dynamics are closely coupled with growth dynamics throughout the growing season (Schiestl-Aalto et al. 2015). Therefore, the integration of phenology and sink activity models should help balance between carbon gain and sink activities in modelling boreal trees' growth. The coupled model of hydraulic eco-physiology and growth should yield outputs that can be directly compared with dendrometer observations without predefined disaggregation.

The model at such a level of complexity often entails numerous parameters, and thus estimating them reasonably and efficiently is particularly important. In this regard, the fast-developing Bayesian techniques serve as remarkable tools, facilitated by prior knowledge provided by earlier modelling and experimental studies.

Model parameterization using Bayesian statistics

Bayesian statistics is a set of techniques that concern expressions of probability distribution and updating the probabilities using new data (Kruschke 2014). This updating process is called model parameterization or calibration (interchangeably) in the current study, which starts with the prior probability distribution of parameter values based on the knowledge *before* the current data and yields the posterior distributions i.e. probabilities of parameter values *given* the current data. According to Bayes' theorem, parameters' posterior probabilities are proportional to the product of their prior probabilities and data distribution i.e. probabilities of the current data given the current parameter values (Gelman et al. 2014). In practice, a Bayesian hierarchical model is commonly constructed, including levels of process, data and (optional) parameter models (Dietze 2017). These levels correspond to the terms in Bayes' theorem as follows. The process and data models are related to the errors between observed and simulated variables, i.e. model outputs ('updated data') given the current parameter values compared with prior observed data. Specifically, process model is the level that formulates the scientific questions and calculates the errors, and it includes the optimal stomata and SRD models in the current study. The data model describes the error probabilities using probability density function(s) (PDF) of error values (often termed likelihood function). The optional level of parameter model describes the prior probability distributions of parameter values, if any of the parameters are not identically and uniformly distributed. Thus, the total probabilities or total likelihood given the current data and parameter values is simply the product of the results of the PDFs in the hierarchical model. This total likelihood is updated after every iteration that samples new parameter values from the prior distributions, until the total likelihood is optimized at the maximum corresponding to the maxima a posteriori (MAP) estimates of the parameters.

Bayesian inference has provided a logically straightforward approach to estimate parameters, and its practical efficiency has been enhanced by recent Markov chain Monte Carlo (MCMC)

especially adaptive MCMC algorithms. In such an algorithm, several parallel simulations ('chains') are started simultaneously, and each of them makes jumps from one sampling point of parameter values to the next following certain rules while also accounting the history of the successful jumps, judging by the consequent marginal change in likelihood (Vrugt et al. 2009; Gelman et al. 2014). Adaptive multi-chain MCMC is considerably more efficient than traditional random walk samplers (e.g. the Metropolis algorithm; Metropolis and Ulam 1949; Metropolis et al. 1953) in seeking the MAP estimates, and the level of convergence can be quantified using between- and within-chain variances (Gelman et al. 2014).

Efficient parameterization techniques helped the current study estimate simultaneously a considerable number of parameters (30—120) of the coupled model with their priors obtained from eco-physiological literature. Consequently, the demand on observed data was reduced, and the coupled model requires only basic meteorological and soil measurement, namely, air temperature, relative humidity, PPFD, and soil water content (or water table depth), besides sap flow and SRD (by dendrometer) for output comparison.

Objectives of the current study

The objectives of the current model development formed a sequence from expanding the optimal stomata model for whole-tree application to coupling it with a cambial growth model, and each step was associated with tests against observations. The steps were

1. Assume optimal hydraulics upstream to stomata and develop a statistical whole-tree model using Bayesian inference (**I**).
2. Based on 1, model semi-mechanistically the hydraulic processes upstream to stomata, including water uptake by roots dependent on soil water content and the conductance between roots and foliage (**II**).
3. Based on 2, model the radial dynamics of tree trunk, including those due to hydraulics and growth simultaneously (**III**).

At all steps the aims also include good performance in tests against observational data.

MODEL FRAMEWORK

Lagrangian optimal stomata model (LOSM)

Cowan and Farquhar (1977) defined stomatal behaviour as optimal when the summed water loss (transpiration) over a given time is minimal with respect to the summed carbon gain (assimilation) over the same period. This definition is equivalent to: If stomatal aperture is perturbed and the integrated perturbation of transpiration rate (E) is non-negative while that of assimilation rate (A) remains zero, then the unperturbed stomatal aperture (i.e. the original state before perturbation) is optimal. That is to say, with perturbed stomatal aperture,

$$\begin{cases} \int \delta E(t)\mathrm{d}t \geq 0 \\ \int \delta A(t)\mathrm{d}t = 0 \end{cases} \tag{4}$$

Taking E as a function of A and rewriting it into an isoperimetric problem, Cowan (1982) expressed the optimality as

$$\int \left[E\big(A(t)\big) - \lambda_{(\mathrm{CF})}A(t)\right]\mathrm{d}t = \text{minimum} \tag{5}$$

where $\lambda_{(\mathrm{CF})}$ is the Lagrange multiplier and the namesake of 'Lagrangian optimal stomata model' (LOSM) to term such models that employ similar mathematical methods of functional analysis. Clearly, $\lambda_{(\mathrm{CF})} = \partial E/\partial A$ at extrema, which lacks an intuitive physiological meaning and is difficult to be compared with experimental results directly. Therefore, Hari et al. (1986) made it inverse, and thus the optimality becomes (with the notation λ retained for convenience)

$$\int [A(t) - \lambda E(t)]\mathrm{d}t = \text{maximum} \tag{6}$$

where λ happens to mean the marginal change of carbon gain per water cost or marginal water use efficiency (MWUE).

The influx of CO_2 follows its own gradient across stomata and is depleted by its photosynthetic use (assimilation, A; Eq. 2). Thus, the dynamics of $\mathcal{C}_\mathrm{i}$ is

$$\dot{\mathcal{C}}_\mathrm{i} \propto g_\sigma(\mathcal{C}_\mathrm{a} - \mathcal{C}_\mathrm{i}) - A \tag{7}$$

while the correlation between A and $\mathcal{C}_\mathrm{i}$ can be linearly approximated (under current ambient $\mathcal{C}_\mathrm{a}$) as

$$A = f(I)\mathcal{C}_\mathrm{i} \tag{8}$$

where $f(I)$ describes foliar reaction to PPFD (I). At equilibrium of $\mathcal{C}_\mathrm{i}$, the stomatal conductance (g_σ^*) fulfils $\dot{\mathcal{C}}_\mathrm{i} = 0$, and from Eq. 7 and 8 it is solved as

$$\mathcal{C}_\mathrm{i}^* = \frac{g_\sigma^*\mathcal{C}_\mathrm{a}}{g_\sigma^* + f(I)} \tag{9}$$

Combine Eq. 3, 6 and 9, and the optimal stomatal behaviour (over an arbitrary period t_1 to t_2) becomes

$$g_\sigma^* = \underset{g_\sigma}{\arg\max} \int_{t_1}^{t_2} \left(\frac{g_\sigma\mathcal{C}_\mathrm{a}}{g_\sigma + f(I)} f(I) - 1.6\lambda g_\sigma D\right)\mathrm{d}t \tag{10}$$

which, solved by applying the Euler-Lagrange equation, is

$$g_\sigma^* = \left(\sqrt{\frac{\mathcal{C}_\mathrm{a}}{1.6\lambda D}} - 1 \right) f(I) \tag{11}$$

where the stomatal reaction to PPFD is

$$f(I) = \frac{\iota\gamma I}{\iota I + \gamma} \tag{12}$$

where ι and γ, respectively, are the initial slope and the asymptote of the curve (Hari and Mäkelä, 2003; Mäkelä et al. 2004). The expression of the optimal stomatal conductance in Eq. 11 and its modifications are frequently used throughout this dissertation and hereafter noted simply as g_σ. The solution of g_σ using $\lambda_{(\mathrm{CF})}$ and following Eq. 5 (cf. Eq. 6) is similar to Eq. 11, but $\lambda_{(\mathrm{CF})}$ would appear within the numerator instead of the denominator of the radicand (e.g. Medlyn et al. 2012).

For more realistic simulations, respiration rate (R), photosynthetic acclimation to air temperature, and the minimum stomatal conductance can be addressed based on the basic LOSM (Eq. 11 and 12; **I**). The respiratory emission of CO_2 offsets $\mathcal{C}_\mathrm{a}$ slightly in the microenvironment surrounding stomata and thus can be incorporated into Eq. 11 as

$$g_\sigma = \left(\sqrt{\frac{\mathcal{C}_\mathrm{a} - R\left(\frac{\iota\gamma I}{\iota I + \gamma}\right)^{-1}}{1.6\lambda D}} - 1 \right) \frac{\iota\gamma I}{\iota I + \gamma} \tag{13}$$

where

$$R = R_0 Q_{10}^{T_\mathrm{l}(T,I)/10} \tag{14}$$

where $T_\mathrm{l}(T,I)$ is leaf temperature (a function of air temperature and PPFD), Q_{10} relative increase of R per 10 °C, and R_0 the value of R at 0 °C (Hari and Mäkelä 2003; Mäkelä et al. 2004). The photosynthetic acclimation to temperature is a key process in boreal trees especially when air temperature fluctuates significantly (e.g. in early spring). This acclimation can be expressed by correlating ι (Eq. 12) and an internal status of the tree (S) instead of taking ι as a time-invariant parameter. The correlation is

$$\iota = \max\{c(S - S_0), 0\} \tag{15}$$

where c is an estimated coefficient when S is higher than a threshold S_0, and the dynamics of S is

$$\dot{S}(t) = \frac{T_\mathrm{l}\big(T(t), I(t)\big) - S(t)}{\tau_S} \tag{16}$$

where τ_S is the time constant of the acclimation and leaf temperature, and leaf temperature (T_l) is a function of air temperature (T) and I (Mäkelä et al. 2004; Kolari et al. 2007). These modifications (Eq. 13—16) took place in **II** and **III**.

Additionally in **III**, the minimum stomatal conductance (g_0) was introduced, which is due to incomplete closure of stomata (Duursma et al. 2019), and its constant value was available from

literature (Heinsoo and Koppel 1999; Hari and Mäkelä 2003). g_0 was used for calculating E (Eq. 3) if $g_0 > g_\sigma$ using Eq. 13. The rest of the model remains the same.

Whole-tree application of LOSM

The current study is based on the 'big-leaf' assumption when expanding LOSM to whole-tree application, that is, regarding a tree crown as a single homogeneous leaf with identical physiological properties. This sacrifice for simplicity may incur higher errors in prediction when in-crown heterogeneity affects the modelled processes (e.g. light extinction on photosynthesis), but the estimated parameters using Bayesian tools still represent well the average properties of the crown, and the detailed sub-models expressing the heterogeneity (e.g. the Beer-Lambert law on light extinction) can be easily implemented subsequently. In practice, an extremely simplistic approach to applying LOSM to whole trees is to assume that water uptake or transport does not limit transpiration or assimilation (e.g. carboxylation efficiency and capacity, and mesophyll conductance), and thus such non-stomatal factors are omitted from the model. This assumption is sensible for a short study period when environmental factors are stable and favourable for the trees. In this case, the parameters of Eq. 11 and 12 can be assumed time-invariant over a period of 8—9 days and directly estimated using a data model (**I**). In the yearly-scale studies on trees under variable temperature, PPFD and soil water conditions, however, non-stomatal limitations on assimilation must be considered. These additional constraints mean that the optimization criterion becomes (cf. Eq. 6)

$$\int \left[A(t) - \Theta\left(E\left(g_\sigma(t)\right), \cdots\right)\right] \mathrm{d}t = \text{maximum} \tag{17}$$

where Θ is the total assimilation deficit (or 'carbon cost') due to transpiration (E) and non-stomatal limitations (e.g. whole-tree water transport and carboxylation capacity). Therefore, the key to expanding LOSM to whole-tree applications is to integrate the non-stomatal limitations with stomatal optimality and thus formulate Θ. Regarding this issue, a thorough work has been undertaken by Dewar et al. (2018; but without waterlogging effects as in the current study), who examined two hypotheses in which, respectively, carboxylation capacity (CC) and mesophyll conductance were associated with reduced leaf water potential due to transpiration. The present study (**II**, **III**) followed their analysis of the CC hypothesis combined with Cowan-Farquhar-style (CF) LOSM to show that Θ can be numerically approximated using λ as a function of whole-tree (i.e. soil-to-leaf) hydraulic conductance (k_{sl}).

Dewar et al. (2018) analysed the CC hypothesis and the CF optimality separately at the beginning. For the CC hypothesis, instead of formulating E, they expressed the water-related costs in A as a linear impact ($\varphi \in [0,1]$) of decreasing leaf water potential ($\psi_{\mathrm{l}} \in [\psi_{\mathrm{A0}}, 0]$, where $\psi_{\mathrm{A0}} < 0$ is a critical value of ψ_{l}) on CC (i.e. CO_2-saturated photosynthetic rate; $\mathcal{V}_{\mathrm{c}}^{\max}$) and 2) an infinite mesophyll conductance so that CO_2 concentration inside chloroplasts equals $\mathcal{C}_{\mathrm{i}}$, Dewar et al. (2018) have demonstrated that at optimal g_σ the net photosynthetically effective intercellular and atmospheric CO_2 concentrations have such a ratio

$$\frac{\mathcal{C}_{\mathrm{i}} - \Gamma^*}{\mathcal{C}_{\mathrm{a}} - \Gamma^*} = \frac{1}{1 + \sqrt{\zeta_{\mathrm{CC}}}} \tag{18}$$

where

$$\zeta_{\mathrm{CC}} = \frac{1.6D\mathcal{V}_{\mathrm{c}}^{\max}}{k_{\mathrm{sl}}|\psi_{\mathrm{A0}}|(\mathcal{M} + \Gamma^*)} \tag{19}$$

where Γ^* is the photorespiratory compensation point, $\mathcal{V}_{\mathrm{c}}^{\max}$ the maximum carboxylation capacity without non-stomatal limitation, k_{sl} soil-to-leaf hydraulic conductance, and $\mathcal{M}$ the Michaelis constant for the Michaelis-Menten kinetics of CO_2. Following a similar analysis but applying CF optimality (Cowan and Farquhar 1977; Cowan 1982) yields

$$\frac{\mathcal{C}_{\mathrm{i}} - \Gamma^*}{\mathcal{C}_{\mathrm{a}} - \Gamma^*} = \frac{1 - \sqrt{\zeta_{\mathrm{CF}} + \frac{1.6\lambda D}{\mathcal{C}_{\mathrm{a}} - \Gamma^*}(1 - \zeta_{\mathrm{CF}})}}{1 - \zeta_{\mathrm{CF}}} \tag{20}$$

where

$$\zeta_{\mathrm{CF}} = \frac{1.6\lambda D}{\mathcal{M} + \Gamma^*} \tag{21}$$

Note that here $\lambda = \lambda_{(\mathrm{CF})}^{-1}$ (*sensu* Hari et al. [1986], Eq. 5 and 6) is used. Thereafter, Dewar et al. (2018) combined the CC hypothesis and the CF optimality by substituting ζ_{CF} in Eq. 20 with

$$\zeta_{\mathrm{CC}} + \zeta_{\mathrm{CF}} = \frac{1.6D(\mathcal{V}_{\mathrm{c}}^{\max} + \lambda k_{\mathrm{sl}}|\psi_{\mathrm{A0}}|)}{k_{\mathrm{sl}}|\psi_{\mathrm{A0}}|(\mathcal{M} + \Gamma^*)} \tag{22}$$

Combined Eq. 20 and 22 can be solved for $\lambda(k_{\mathrm{sl}})$, and the result is

$$\lambda = \frac{(\mathcal{M} + \Gamma^*)(\mathcal{C}_{\mathrm{a}} - \mathcal{C}_{\mathrm{i}})^2}{1.6yD} + \frac{\mathcal{V}_{\mathrm{c}}^{\max}(\mathcal{C}_{\mathrm{i}} - \Gamma^*)^2}{k_{\mathrm{sl}}|\psi_{\mathrm{A0}}|y} \tag{23}$$

where

$$y = \mathcal{C}_{\mathrm{i}}^2 + \Gamma^*(\mathcal{C}_{\mathrm{a}} - 2\mathcal{C}_{\mathrm{i}}) + \mathcal{M}(\mathcal{C}_{\mathrm{a}} - \Gamma^*) \tag{24}$$

Eq. 23 shows that λ and k_{sl} are approximately inversely correlated. Hence, for a simpler practice, the correlation may be approximated by (Hölttä et al. 2017)

$$\lg \lambda = z_0 + z_1 \lg\left(\frac{k_{\mathrm{sl}}}{k_0}\right) \tag{25}$$

where k_0 is the base-case xylem conductance without embolism, and z_0 and z_1 coefficients (both negative). This approximation performs well within the reasonable range of k_{sl} (Figure 1). Combine Eq. 25 and $\lambda = \partial A/\partial E = \partial\Theta/\partial E$ (Wolf et al. 2016), integrate over E, and there is

$$\Theta = 10^{z_0}\left(\frac{k_{\mathrm{sl}}}{k_0}\right)^{z_1} E(g_\sigma) \tag{26}$$

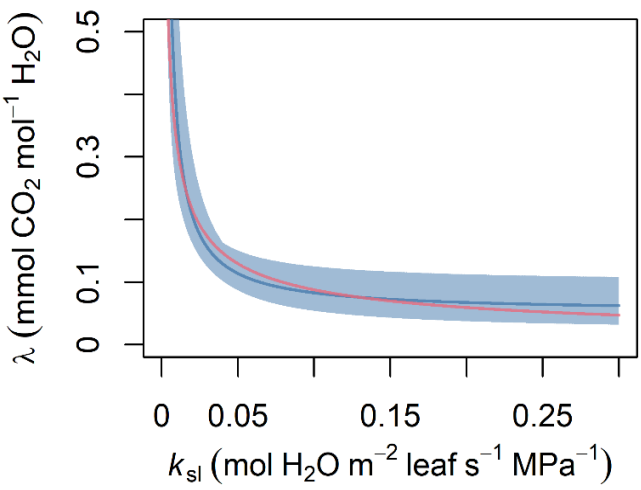

Figure 1 The analytic expression of $\lambda(k_{sl})$ (Eq. 23 and 24, blue shade corresponding to $\mathcal{C}_i/\mathcal{C}_a \in [0.5,0.7]$ and blue line the shade's mean) and its numerical approximation (Eq. 25, pink line). For Eq. 23 and 24, $\mathcal{M}$ = 11.153 × 10^{-6} mol mol^{-1} (Galmés et al. 2016), $\mathcal{V}_c^{max}$ = 8.75 × 10^{-6} mol m^{-2} s^{-1} (Kellomäki and Wang 1996), *D* the mean of observations in **II**, and $\mathcal{C}_a$, Γ^* and ψ_{A0} as of Dewar et al. (2018). For Eq. 25, z_0 = -3.69, z_1 = -0.56, which are within their respective prior ranges in **III**.

which numerically approximates the total assimilation deficit due to stomatal behaviour (g_σ), whole-tree xylem transport (k_{sl}), and non-stomatal constraints on assimilation ($\mathcal{V}_c^{max}$, $\mathcal{M}$, and Γ^*).

Take k_{sl} as a series of two components, soil-to-root (k_{sr}) and root-to-leaf (k_{rl}) conductances, and thus

$$k_{sl}^{-1} = k_{sr}^{-1} + k_{rl}^{-1} \tag{27}$$

Empirically, a tree's k_{rl} can be estimated using the maxima of its sap flow density (J) and the difference between soil (ψ_s) and leaf water potentials (Duursma et al. 2008; Martínez-Vilalta et al. 2009), i.e.

$$k_{rl} = \frac{\max\{J(t)\}}{\rho_{lw} \max\{|\psi_s - \psi_l|\}} \tag{28}$$

where ρ_{lw} is all-sided leaf to sapwood area ratio for converting k_{rl} to be per leaf area and thus in accordance with E's unit. Under low to medium water contents, k_{sr} is typically in a positive correlation with (volumetric) soil water content (SWC, θ), which can be modelled via ψ_s as (Duursma et al. 2008)

$$k_{sr}^{+}(\psi_s) = \frac{2\pi\rho_{rl}}{\ln \rho_{rr}} K_{sat} \left(\frac{\psi_e}{\psi_s}\right)^{2+\frac{3}{b}} \tag{29}$$

where ρ_{rl} and ρ_{rr} are root length to all-sided leaf area and rhizosphere to mean hydraulically active root diameters ratios, respectively, K_{sat} saturated soil hydraulic conductivity, ψ_e soil water potential of air entry, b a coefficient related to the soil retention curve (Newman 1969; Campbell 1974), and

$$\psi_s^{mineral} = \psi_e \left(\frac{\theta}{\theta_{sat}}\right)^{-b} \tag{30}$$

where θ_{sat} is saturated SWC (Clapp and Hornberger 1978; Cosby et al. 1984; Duursma et al. 2008). Thus, Eq. 29 and 30 may be combined and simplified to

$$k_{sr}^{mineral} = k_{sr}^{+}(\theta) = \xi_m \left(\frac{\theta}{\theta_{sat}}\right)^{\xi_p} \quad (31)$$

where ξ_m and ξ_p are coefficients lumped from Eq. 29 and 30. This form of power function has been supported by experimental observation (Poyatos et al. 2018) and was used for modelling k_{sr} of mineral soils in the current study.

Waterlogging effects of excess SWC on k_{sr} lacked direct observation for continuous quantification. Nevertheless, in experiment it has been found that the decline in belowground conductance relative to optimal SWC due to drought and flooding treatments is of a similar degree (Domec et al. 2021). Additionally, existing models on oxygen diffusivity in soil are generally in the form of power function as well (e.g. Penman 1940; Moldrup et al. 1996). Therefore, a form algebraically symmetrical to Eq. 31 was designed to reflect the negative correlation between k_{sr} and SWC ($k_{sr}^{-}(\theta)$) with utilizing the information on available soil porosity for gases ($1 - \theta/\theta_{sat}$) and optimal SWC (θ^*) (**II**), that is,

$$k_{sr}^{-}(\theta) = \eta_m \left(\frac{2\theta^* - \theta}{\theta_{sat}}\right)^{\eta_p} \quad (32)$$

where η_m and η_p are coefficients that should fall into similar value ranges of ξ_m and ξ_p (Eq. 31), respectively. Then, a 'plateau' segment or the optimal k_{sr} ($k_{sr}^{*}(\theta^*)$) connects the curves of k_{sr}^{+} and k_{sr}^{-} such that it covers a prescribed range of water table depth (WTD; e.g. 15 cm [**III**] or 20 cm [**II**] according to prior knowledge, and WTD can be converted to SWC using Eq. 51). Finally, the overall $\underline{k}_{sr}(\theta)$ in peatland is determined by

$$k_{sr}^{peat} = \min\{k_{sr}^{+}, k_{sr}^{-}, k_{sr}^{*}\} \quad (33)$$

Stem radial dimension (SRD) model

SRD in the current model refers to tree's diameter (DBH) or radius (RBH) at breast height (l_{BH}), of which the dynamics are due to reversible elastic changes and irreversible growth (**III**), i.e.

$$\dot{l}_{BH} = \dot{l}_{ela} + \dot{l}_{gro} \quad (34)$$

where $\dot{l}_{ela}$ is driven by the dynamics of water potential at breast height via the (linear) modulus of elasticity (MOE, $\mathcal{E}$). When the water potentials of xylem and cambium are assumed to equilibrate instantly and cambial osmotic potential (ψ_{Π}^{cam}) is assumed constant, the dynamics of turgor pressure of the cambium at breast height ($\dot{\psi}_{p}^{cam}$) can be used for modelling $\dot{l}_{ela}$ instead of the total water potential dynamics, as $\dot{\psi}^{xylem} = \dot{\psi}^{cam} = \dot{\psi}_{p}^{cam} + \dot{\psi}_{\Pi}^{cam} + \dot{\psi}_{g}^{cam}$ and $\dot{\psi}_{\Pi}^{cam} = 0$, $\dot{\psi}_{g}^{cam} = 0$ (gravitational potential). Hence

$$\dot{l}_{\mathrm{ela}} = \frac{\dot{\psi}_{\mathrm{p}}^{\mathrm{cam}}}{\mathcal{E}} l_0 \tag{35}$$

where l_0 is the initial value of l_{BH}. The assumption of constant $\psi_{\Pi}^{\mathrm{cam}}$ is based on field observations on boreal conifers (Paljakka et al. 2017) and previous practice using a similar model (Cabon et al. 2020). The water potential at breast height in the xylem can be estimated using ψ_{s} and the sap flow ($J^{(\mathrm{O})}$) and conductance (k_{sb}) between soil and breast height, analogous to Ohm's law for an electrical network. Thus,

$$\dot{\psi}^{\mathrm{cam}}(t) = \dot{\psi}_{\mathrm{p}}^{\mathrm{cam}}(t) = \dot{\psi}^{\mathrm{xylem}}(t) = \dot{\psi}_{\mathrm{s}}(t) - \frac{\mathrm{d}}{\rho_{\mathrm{lw}} \mathrm{d}t}\left(\frac{J^{(\mathrm{O})}(t)}{k_{\mathrm{sb}}(t)}\right) \tag{36}$$

Note, again, that gravitational potential difference between soil and breast height is time-invariant and thus cancelled from the right-hand side of Eq. 36 by the differentiation with respect to time. ψ_{s} can be estimated for mineral soils using Eq. 30 and for peat using (van Genuchten 1980; Hallema et al. 2015)

$$\psi_{\mathrm{s}}^{\mathrm{peat}}(\theta) = -\left[\frac{\left(\frac{\theta - \theta_{\mathrm{res}}}{\theta_{\mathrm{sat}} - \theta_{\mathrm{res}}}\right)^{-4.4248} - 1}{0.0231}\right]^{0.774} \quad (\mathrm{cm}) \times 98.2\ (\mathrm{Pa\ cm^{-1}}) \tag{37}$$

The soil-to-breast height conductance k_{sb} in Eq. 36, similar to Eq. 27, follows

$$k_{\mathrm{sb}}^{-1} = k_{\mathrm{sr}}^{-1} + k_{\mathrm{rb}}^{-1} \tag{38}$$

where k_{sr} is the same as in LOSM (Eq. 29—32). The root-to-breast height conductance (k_{rb}) relative to k_{rl} is correlated with the distance between roots (the average depth where water uptake is the most active) and breast height (h_{rb}) relative to root-to-leaf hydraulic transport distance (h_{rl}). This correlation is derived from the correlation between hydraulic conductivity (K) and transport distance, $K \propto \sqrt{h}$ (Nikinmaa et al. 2014), and the definition of k using K, $k \overset{\mathrm{def}}{=} \mathrm{d}K/\mathrm{d}h$. Hence,

$$\frac{k_{\mathrm{rb}}}{k_{\mathrm{rl}}} = \sqrt{\frac{h_{\mathrm{rl}}}{h_{\mathrm{rb}}}} \tag{39}$$

and thus the conductances in Eq. 38 can be evaluated using tree height.

Although the assumption $\dot{\psi}^{\mathrm{xylem}} = \dot{\psi}^{\mathrm{cam}}$ is good when xylem is the sole water source for cambium, noticeable expansion and contraction of l_{BH} associated with rain events were observed in **III** without corresponding signals in SWC or WTD, suggesting rainwater uptake possibly through lenticels which became an additional water input of cambium. Therefore, the pressure potential difference between bark and cambium ($\Delta\psi_{\mathrm{bc}}$) water in the bark was incorporated into $\dot{\psi}_{\mathrm{p}}^{\mathrm{cam}}$ based on Eq. 36. The bark was analysed as an 'RC (resistor-capacitor) circuit' embodying hydraulic capacitance (C_{b}) and conductance between bark and cambium (k_{bc}), charged by rainwater (u_{bin}) and discharged by cambium (u_{bc}). The definitions of $C_{\mathrm{b}} \overset{\mathrm{def}}{=} \partial q_{\mathrm{b}}/\partial(\Delta\psi_{\mathrm{bc}})$ and bark MOE $\mathcal{E}_{\mathrm{b}} \overset{\mathrm{def}}{=} \partial(\Delta\psi_{\mathrm{bc}})/(\partial l_{\mathrm{b}}/l_{\mathrm{b0}})$ can be combined by expressing q_{b} as bark water quantity per bark area (i.e. a 'thickness' in e.g. mm) and thus $\partial q_{\mathrm{b}} \equiv \partial l_{\mathrm{b}}$. Hence,

$$C_{\mathrm{b}} \overset{\text{def}}{=} \frac{\partial q_{\mathrm{b}}}{\partial(\Delta\psi_{\mathrm{bc}})} = \frac{\mathrm{d}q_{\mathrm{b}}/\mathrm{d}t}{\mathrm{d}(\Delta\psi_{\mathrm{bc}})/\mathrm{d}t} = \frac{l_{\mathrm{b0}}}{\mathcal{E}_{\mathrm{b}}} \tag{40}$$

and thus, at any time point t_x within the study period, the marginal change of $\Delta\psi_{\mathrm{bc}}$ is

$$\begin{aligned} \frac{\mathrm{d}\big(\Delta\psi_{\mathrm{bc}}(t_x)\big)}{\mathrm{d}t} &= \frac{\dot{q}_{\mathrm{b}}(t_x)}{C_{\mathrm{b}}} = \frac{u_{\mathrm{bin}}(t_x) - u_{\mathrm{bc}}(t_x)}{l_{\mathrm{b0}}/\mathcal{E}_{\mathrm{b}}} \\ &= \left[u_{\mathrm{bin}}(t_x) - \frac{\mathcal{E}_{\mathrm{b}} k_{\mathrm{bc}}}{l_{\mathrm{b0}}} \int_0^{t_x} \dot{q}_{\mathrm{b}}(t)\mathrm{d}t\right] \frac{\mathcal{E}_{\mathrm{b}}}{l_{\mathrm{b0}}} \end{aligned} \tag{41}$$

Note that the initial state $q_{\mathrm{b}}(0) = 0$ and thus $q_{\mathrm{b}}(t_x) \equiv \int_0^{t_x} \dot{q}_{\mathrm{b}}(t)\mathrm{d}t$. The water input is given by

$$u_{\mathrm{bin}}(t) = \min\{\wp(t), u_{\mathrm{bin}}^{\max}\} \tag{42}$$

and the maximum value $u_{\mathrm{bin}}^{\max}$ was evaluated experimentally (Gimeno et al. 2022). $\mathrm{d}(\Delta\psi_{\mathrm{bc}})/\mathrm{d}t$ is added to Eq. 36 to include rainwater effects in $\dot{\psi}_{\mathrm{p}}^{\mathrm{cam}}$, i.e.

$$\dot{\psi}^{\mathrm{cam}}(t) = \dot{\psi}_{\mathrm{p}}^{\mathrm{cam}}(t) = \dot{\psi}_{\mathrm{s}}\big(\theta(t)\big) - \frac{\mathrm{d}}{\rho_{\mathrm{lw}}\mathrm{d}t}\left(\frac{J(t)}{k_{\mathrm{sb}}(t)}\right) + \frac{\mathrm{d}\big(\Delta\psi_{\mathrm{bc}}(t)\big)}{\mathrm{d}t} \tag{43}$$

which is used in Eq. 35.

The model of growth dynamics ($\dot{l}_{\mathrm{gro}}$ in Eq. 34) is based on a sink limitation growth model focussed on enzymatic activation of cambium (Johnson et al. 1942; Parent et al. 2010; Cabon et al. 2020). The key environmental factors of the sink activities are temperature (T) and turgor at the place of interest (breast height in the current study) (Lockhart 1965). As the model is aimed at capturing the dynamics of cell number or SRD, it simulates only the enlargement phase of xylogenesis while disregarding the other phases (e.g. wall thickening) that have little impact on cell number or SRD. It is assumed that a cambial cell's volume (V) must double before a new cell is generated by splitting. Thus, from the macroscopic perspective, growth within an arbitrary period t_1 to t_2 can be formulated by counting the number of times of cambial cell doubling (N_{D}) within the period, which is

$$N_{\mathrm{D}} = \log_2 \frac{V(t_2)}{V(t_1)} = \frac{\ln V(t_2) - \ln V(t_1)}{\ln 2} = \frac{1}{\ln 2}\int_{t_1}^{t_2} \frac{\dot{V}(t)}{V(t)}\mathrm{d}t \tag{44}$$

Define the *linear* (as opposed to *volumetric*, for the consistency of the current model framework, e.g. Eq. 43) cell expansion rate as $g \overset{\text{def}}{=} \dot{d}_{\mathrm{c}}/d_{\mathrm{c}} = \big(\dot{V}/V\big)/3$ (d_{c}, radial diameter of cambial cell), assuming the relative expansion rate identical on all the three dimensions of the cell. Introduce g into Eq. 44, upscale it to the whole cambium, and the growth rate becomes

$$\dot{l}_{\mathrm{gro}} = N_{\mathrm{c}}\dot{N}_{\mathrm{D}}\bar{d}_{\mathrm{c}} = N_{\mathrm{c}}\frac{g}{\ln 2}\bar{d}_{\mathrm{c}} \tag{45}$$

where N_{c} is the number of active cambial cells in one radial file, $\bar{d}_{\mathrm{c}}$ the average d_{c}, and g is driven by turgor ($\psi_{\mathrm{p}}^{\mathrm{cam}}$) and temperature over respective thresholds (Lockhart 1965). However, to avoid

uncertainties in estimating $\psi_{\Pi}^{\mathrm{cam}}$ and be consistent with the previous modelling work (Cabon et al. 2020), threshold $\psi_{\mathscr{g}0}$ is set on total water potential at breast height (ψ^{cam}) instead of $\psi_{\mathrm{p}}^{\mathrm{cam}}$, Thus,

$$\mathscr{g} = \begin{cases} \phi(T) \cdot \left(\psi^{\mathrm{cam}} - \psi_{\mathscr{g}0}\right), & \psi^{\mathrm{cam}} \geq \psi_{\mathscr{g}0} \\ 0, & \psi^{\mathrm{cam}} < \psi_{\mathscr{g}0} \end{cases} \tag{46}$$

where $\psi^{\mathrm{cam}} = \int \dot{\psi}^{\mathrm{cam}}(t)\mathrm{d}t - \Delta\psi_{\mathrm{g}}$ using Eq. 43 ($\Delta\psi_{\mathrm{g}}$, gravitational potential difference between soil and breast height). Note that $\left(\psi^{\mathrm{cam}} - \psi_{\mathscr{g}0}\right)$ is still the difference in turgor as $\psi_{\Pi}^{\mathrm{cam}}$ is assumed constant. When $T \geq T_0$ (the threshold temperature), the linear cell wall extensibility ($\phi(T)$) in Eq. 46 depends on the characteristics of the trees' enzymatic system, namely, the enthalpy of activation (ΔH_{a}) and the enthalpy (ΔH_{d}) and entropy (ΔS_{d}) differences between the active and inactive states. It is formulated as

$$\phi(T) = \begin{cases} \phi_{\max} \dfrac{\alpha(T + 273.15)\exp\left(\dfrac{\Delta H_{\mathrm{a}}}{8.3145\ (T + 273.15)}\right)}{1 + \exp\left[\dfrac{\Delta S_{\mathrm{d}}}{8.3145}\left(1 - \dfrac{\Delta H_{\mathrm{d}}}{\Delta S_{\mathrm{d}}(T + 273.15)}\right)\right]}, & T \geq T_0 \\ 0, & T < T_0 \end{cases} \tag{47}$$

where α is a scaling coefficient such that $\phi(303.15\ \mathrm{K}) = \phi_{\max}$.

Despite the growth model's biological basis (Johnson et al. 1942) and its tests on temperate crops and trees (Parent and Tardieu 2012; Cabon et al. 2020), its applicability to boreal forests was uncertain. The strong phenology driven by temperature and water conditions (Kramer et al. 2000; Delpierre et al. 2016a) may suppress sink activities via carbon availability due to the low net primary production (NPP; Cramer et al. 1999). Therefore, a module accounting for the seasonality of N_{c} was added in the current study (**III**). It has been found that N_{c} during growing season can be described well by the derivative of the Gompertz function (Cuny et al. 2013). Here it takes the form

$$N_{\mathrm{c}}(t) = N_{\mathrm{c}}^{\max} \frac{m\mathcal{T}}{\tau_{\mathrm{G}}} \exp\left[-m \exp\left(-\frac{t}{\tau_{\mathrm{G}}}\right) - \frac{t}{\tau_{\mathrm{G}}}\right] \tag{48}$$

where m and τ_{c} are the displacement and (inverse) rate parameters, respectively, $N_{\mathrm{c}}^{\max}$ the maximum value of N_{c} (evaluated as the constant N_{c} given by Cabon et al. [2020]), and the time unity $\mathcal{T}$ (e.g. 1 h) is to unify the unit of the equation. Substitute N_{c} in Eq. 43 with Eq. 46, and thus

$$\dot{l}_{\mathrm{gro}} = N_{\mathrm{c}}^{\max} \frac{m\mathcal{T}}{\tau_{\mathrm{c}}} \exp\left[-m \exp\left(-\frac{t - t_0}{\tau_{\mathrm{c}}}\right) - \frac{t - t_0}{\tau_{\mathrm{c}}}\right] \cdot \frac{\mathscr{g}}{\ln 2} \bar{d}_{\mathrm{c}} \tag{49}$$

The entire formulation hereby is referred to as full model (FM), and its simulation of SRD was compared with that of two alternative models (AMs) for testing the necessity of the Gompertz function (Eq. 46). AM1 uses only the mechanistic model of enzyme metabolism and cell expansion for simulating $\dot{d}_{\mathrm{gro}}$ without Eq. 48 and, to the contrary, AM2 uses only Eq. 48 without the mechanistic model. Hence, in AM1 $N_{\mathrm{c}}^{(\mathrm{AM1})} \equiv N_{\mathrm{c}}^{\max}$ in Eq. 45, and in AM2 the mechanistic model of growth (Eq. 46 and 47) is not used, $\left(\psi^{\mathrm{cam}} - \psi_{\mathscr{g}0}\right)$ is set to 1 MPa constantly for arithmetic

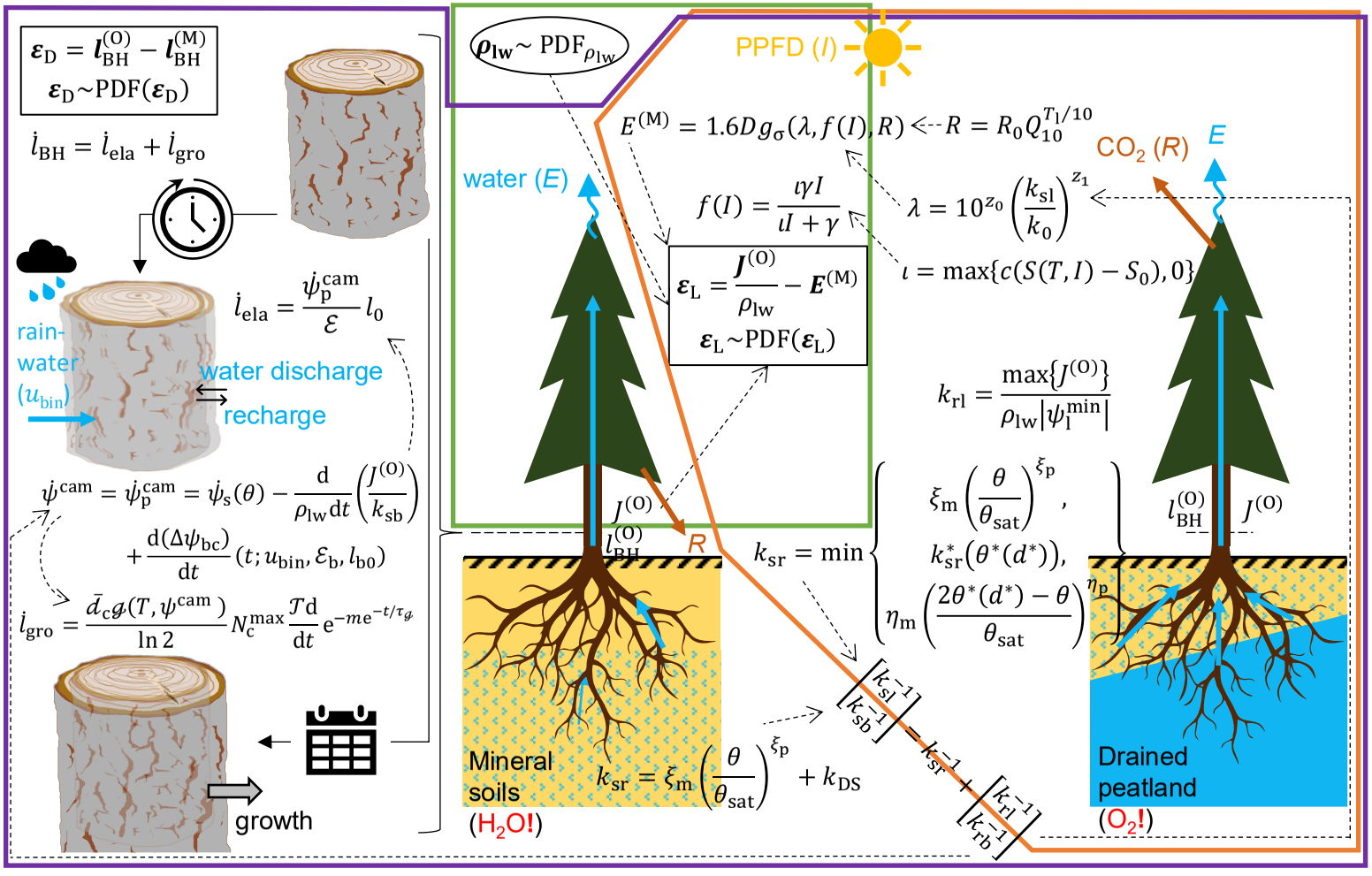
$\varepsilon_D = l_{BH}^{(O)} - l_{BH}^{(M)}$
$\varepsilon_D \sim \mathrm{PDF}(\varepsilon_D)$
$\dot{l}_{BH} = \dot{l}_{ela} + \dot{l}_{gro}$
rain-water (u_{bin})
water discharge
recharge
$\dot{l}_{ela} = \frac{\dot{\psi}_p^{cam}}{\varepsilon} l_0$
$\dot{\psi}^{cam} = \dot{\psi}_p^{cam} = \dot{\psi}_s(\theta) - \frac{d}{\rho_{lw} dt}\left(\frac{J^{(O)}}{k_{sb}}\right) + \frac{d(\Delta\psi_{bc})}{dt}(t; u_{bin}, \mathcal{E}_b, l_{b0})$
$\dot{l}_{gro} = \frac{\bar{d}_c \mathcal{G}(T, \psi^{cam})}{\ln 2} N_c^{max} \frac{\mathcal{T} d}{dt} e^{-m e^{-t/\tau_g}}$
growth
$\rho_{lw} \sim \mathrm{PDF}_{\rho_{lw}}$
PPFD (I)
$E^{(M)} = 1.6 D g_\sigma(\lambda, f(I), R)$
$R = R_0 Q_{10}^{T_l/10}$
$f(I) = \frac{\iota\gamma I}{\iota I + \gamma}$
$\lambda = 10^{z_0}\left(\frac{k_{sl}}{k_0}\right)^{z_1}$
$\iota = \max\{c(S(T,I) - S_0), 0\}$
$\varepsilon_L = \frac{J^{(O)}}{\rho_{lw}} - E^{(M)}$
$\varepsilon_L \sim \mathrm{PDF}(\varepsilon_L)$
water (E)
CO_2 (R)
E
$k_{rl} = \frac{\max\{J^{(O)}\}}{\rho_{lw}|\psi_l^{min}|}$
$k_{sr} = \min\left\{\xi_m\left(\frac{\theta}{\theta_{sat}}\right)^{\xi_p}, k_{sr}^*(\theta^*(d^*)), \eta_m\left(\frac{2\theta^*(d^*) - \theta}{\theta_{sat}}\right)^{\eta_p}\right\}$
$J^{(O)}$
$l_{BH}^{(O)}$
R
$k_{sr} = \xi_m\left(\frac{\theta}{\theta_{sat}}\right)^{\xi_p} + k_{DS}$
$k_{sl}^{-1}, k_{sb}^{-1}, k_{sr}^{-1}, k_{rl}^{-1}, k_{rb}^{-1}$
Mineral soils
(H_2O!)
Drained peatland
(O_2!)

Figure 2 (facing page) Schematic framework of the models. See *Symbols* and *Modelling framework* for details of the symbols and equations. The green, orange and purple frames are the scopes of **I**, **II** and **III**, and black squares and circle are data and parameter models, respectively.

convenience, and thus $g^{(\mathrm{AM2})} \equiv \phi^{\max} \cdot 1\,\mathrm{MPa}$ in Eq. 49 where $\phi^{\max}$ is still an estimated parameter. The rest of the model structure and parameterization method remained the same as for FM.

Data and parameter models

In **I** and **II**, the process model is the whole-tree LOSM and calculates the error ($\boldsymbol{\varepsilon}_{\mathrm{L}}$) between modelled transpiration rate ($\boldsymbol{E}^{(\mathrm{M})}$, using Eq. 3 with optimal g_σ by Eq. 11[**I**] or 13 [**II**]) and observed sap flow density ($\boldsymbol{J}^{(\mathrm{O})}$) per leaf area, i.e. $\boldsymbol{\varepsilon}_{\mathrm{L}} = \boldsymbol{J}^{(\mathrm{O})}/\rho_{\mathrm{lw}} - \boldsymbol{E}^{(\mathrm{M})}$. In **III**, the process model includes the whole-tree LOSM and the SRD model, each of which has its own error matrix, i.e. $\boldsymbol{\varepsilon}_{\mathrm{L}}$ defined the same as in **II**, and $\boldsymbol{\varepsilon}_{\mathrm{D}} = \boldsymbol{l}_{\mathrm{BH}}^{(\mathrm{O})} - \boldsymbol{l}_{\mathrm{BH}}^{(\mathrm{M})}$ (for each tree and each year if multiple-year data were available, $l_{\mathrm{BH}}(t_x) = \int_0^{t_x} \dot{l}_{\mathrm{BH}}(t)\mathrm{d}t$ for any time point t_x within the study period. When the temporal scale of study was finer than a day (**I**, **III**), a time lag (χ) was introduced into the calculation of $\boldsymbol{\varepsilon}_{\mathrm{L}}$ to account for the time difference between the dynamics of $\boldsymbol{J}^{(\mathrm{O})}$ and $\boldsymbol{E}^{(\mathrm{M})}$ mainly due to water storage in the tree (but see Hölttä et al. [2015] for the effects on χ associated with the method of sap flow measurement). In this case, either χ was a parameter directly estimated (**I**) or the proportion between χ and tree height h (**III**; i.e. the β in $\chi = \beta h$, according to a finding in **I**) was an estimated parameter.

Data models include the PDFs of $\boldsymbol{\varepsilon}_{\mathrm{L}}$ (**I**, **II**, **III**) and $\boldsymbol{\varepsilon}_{\mathrm{D}}$ (**III**), and in **III** the total product of the two PDFs' results was maximized. A parameter model is present in **I** to describe the distribution of ρ_{lw} related to tree age/size (McDowell et al. 2002), whereas ρ_{lw} in **II** and **III** was not a parameter but calculated using measured h, DBH (Repola 2009) and specific leaf area (SLA). In **II** and **III**, all the parameters were assumed independently and uniformly distributed *a priori*, and thus parameter model is absent therein. The PDF of the normal (Gaussian; **II**), Laplace (**I**, **III**) and heavy-tailed Gaussian (**I**; Sivia and Skilling 2006) distributions were selected for the data and parameter models, according to prior knowledge and pilot runs using default parameter values.

The scheme of the modelling framework is presented in Figure 2.

MATERIALS AND METHODS

Study sites and sample trees

The study sites were at Hyytiälä Forest Station, Juupajoki (**I**, **III**), Sattasuo, Rovaniemi (**II**), and Ränskälänkorpi, Asikkala (**III**), Finland (Table 1). The studied trees were of the dominant species Scots pine (*Pinus sylvetris* L.) at Hyytiälä and Sattasuo and Norway spruce (*Picea abies* (L.) H. Karst.) at Ränskälänkorpi (Table 2). At Hyytiälä for **I**, the plots of young (age < 60 years) and old

(age > 130 years) Scots pine trees were in different site types (VT vs OMT/MT; *sensu* Lehto 1964) and with a distance of *c*. 500 m in between. For **III** two trees were selected from the stand close to the young plot of **I**. Sattasuo and Ränskälänkorpi are peatland drained by ditches since *c.* 1960's. In March 2021 before the growing season began, selection harvest was undertaken at a block of forest (selection harvest block, SHB) at Ränskälänkorpi to render the basal-area density of Norway spruce to 12.0 m^2 ha^{-1} vs 35.8 m^2 ha^{-1} in the control block (CB). SBH and CB were *c*. 190-m distant from each other but of the same site type (MT) (Laurila et al. 2021).

Table 1 Information on study sites.

Name	Hyytiälä (**I**, **III**)	Sattasuo (**II**)	Ränskälänkorpi (**III**)
Coordinates	61.8°N, 24.3°E	66.5°N, 26.7°E	61.2°N, 25.3°E
Landscape	Coniferous forest	Wooded drained peatland	Wooded drained peatland
Mean summer temperature (°C)	15.15 (June—July, 2009—2018)	15.0 (July, 1981—2010)	16.6 (July, 1981—2010)
Mean precipitation (mm yr^{-1})	190.9 (June—July, 2009—2018)	505 (annual, 1981—2010)	600 (annual, 1981—2010)
Site type[a] / productivity	OMT/MT (**I**) VT (**I**, **III**)	Medium	MT
Dominant tree species (DTS)	*Pinus sylvestris*	*P. sylvestris*	*Picea abies*
DTS density[b]	--	91 m^3 ha^{-1}	12.0 m^2 ha^{-1} (thinned), 35.8 m^2 ha^{-1} (control)
Study period	9—27 July 2018 (**I**) 2015—2019 (**III**)	2008—2011	March—September 2021
Time resolution of study	10 min (**I**) 30 min (**III**)	1 day	30 min
Reference	Hari and Kulmala (2005)	Stenberg et al. (2018)	Laurila et al. (2021)

[a] Site type: OMT, *Oxalis-Vaccinium myrtillus* type (mesic and productive); MT, *V. myrtillus* type (mesic); VT, *V. vitis-idaea* type (sub-xeric).
[b] Note the difference in expression between **II** (wood volume density, m^3 ha^{-1}) and **III** (basal area density, m^2 ha^{-1}).

Table 2 Information on the sample trees. For Hyytiälä (**III**) the properties of the trees at the beginning (2015) and the end (2019) of study period are shown, while elsewhere the value ranges of all sample trees are displayed. DBH, diameter at breast height; sd, standard deviation; Y, young; O, old; C, control; Th, thinned.

Site	Hyytiälä (**I**)	Hyytiälä (**III**)	Sattasuo (**II**)	Ränskälänkorpi (**III**)
Species	*Pinus sylvestris*	*P. sylvestris*	*P. sylvestris*	*Picea abies*
Number of trees	5 (Y) + 6 (O)	2 ("P" & "S")	6	4 (C) + 7 (Th)
Age at study time (mean ± sd) (year)	Y: 50—52 (51 ± 1.0) O: 132—177 (149 ± 16.5)	*c.* 50—55	66—87	C: 43—78 (63.3 ± 16.0) Th: 47—87 (60.4 ± 15.3)
Height (mean ± sd) (m)	Y: 16.0—20.9 (18.5 ± 1.7) O: 31.0—36.8 (34.3 ± 1.9)	P: 17.9—19.2 S: 18.4—19.7	11.2—14.0 (12.2 ± 1.1)	C: 13.6—22.2 (16.4 ± 3.9) Th: 10.9—23.3 (17.1 ± 4.4)
DBH (mean ± sd) (cm)	Y: 17.3—23.9 (20.9 ± 2.4) O: 43.0—51.5 (47.7 ± 2.6)	P: 22.3—23.8 S: 21.8—22.9	12.9—17.5 (15.1 ± 1.6)	C: 12.1—28.0 (17.5 ± 7.2) Th: 9.5—26.1 (17.1 ± 5.9)

Sap flow measurement

At Hyytiälä (**I**, **III**) and Sattasuo (**II**), sap flow density of the sample trees was measured by the thermal dissipation method (Granier 1987; Lu et al. 2004). One (**II**, **III**) or four (**I**) pair(s) of *c.* 3.5-cm-long Type T thermocouple probes, one heated (HP) and the other reference (RP) in each pair, were mounted to each sample tree at breast height (*c.* 1.3 m from the ground) on its north side (**II**) or four ordinal directions (NW, SW, SE, NE; **I**). In all cases, RP was directly below HP by *c.* 10 cm, and the constant heating power to each HP was 0.2 W. All the probes were protected by aluminium foil or boxes with ventilation holes.

The voltage difference (ΔU) between HP and RP was measured every half (**I**) or one minute (**II**, **III**) and averaged and recorded every 10 min. The raw sap flow density (mol m^{-2} s^{-1}, converted from m s^{-1}) was calculated using (Lu et al. 2004)

$$J^{(\mathrm{O})} = 118.99 \times 10^{-6} \left(\frac{\Delta U^* - \Delta U}{\Delta U} \right)^{1.231} \cdot \frac{10^6 \text{ g m}^{-3}}{18.01528 \text{ g mol}^{-1}} \tag{50}$$

where the baseline voltage difference (ΔU^*) was determined according to the criteria given by Baseliner 4.0 (Oishi et al. 2008; Oishi et al. 2016). The raw results of Eq. 50 were adjusted by sapwood depths of the trees (**I**, **II**; Clearwater et al. 1999; Berdanier et al. 2016) and area fractions of the four directions (**I**).

At Ränskälänkorpi (**III**), sap flow density was measured using heat pulse velocity sap flow and water content sensors (HPV-06, Implexx Sense, Australia). Mounted on the trees' south side at breast height, each sensor comprises three 30-mm-long probes, two heated with the other reference in the middle, with a 6-mm distance between each two. The sensors were covered similarly as in **I** and **II**. Temperature differences at 10 mm (inner in the xylem) and 20 mm (outer) from the probes' tips following heat pulse were recorded every 15 min and converted to sap flow rate (L h^{-1}) using the built-in species- specific calibration of the device. The average of the inner and outer readings was used for calculating $J^{(O)}$ per measured sapwood area at breast height.

Environmental variables

Air temperature, relative humidity, and PPFD data were collected from the system of Stations for Measuring Forest Ecosystem-Atmosphere Relations (SMEAR) for Hyytiälä (**I**, **III**) or measured at the sites at Sattasuo (**II**) and Ränskälänkorpi (**III**). At Sattasuo and Ränskälänkorpi, WTD was recorded automatically within evenly distributed plastic tubes into the ground around the sample trees (Intech Instruments Ltd, Dataflow Systems Ltd, New Zealand), supplemented with occasional manual measurement. During modelling, WTD (d) was converted to SWC (θ) using

$$\theta = \theta_{\mathrm{res}} + \frac{\theta_{\mathrm{sat}} - \theta_{\mathrm{res}}}{[1 + (0.072\ d)^{1.371}]^{1-1.371^{-1}}} \tag{51}$$

where θ_{res} is the residual SWC (van Genuchten 1980; Leppä et al. 2020; **II**, **III**).

The time resolutions of the environmental data were unified with the respective sap flow measurements at Hyytiälä and Ränskälänkorpi (**I**, **III**; Table 1) by averaging the variables in finer time resolutions. VPD was calculated from air temperature and relative humidity before the averaging. At Sattasuo (**II**), the median of the maxima 10% by ranking of each day was extracted as daily-level data of the environmental variables as well as sap flow density before applying them to the model. In the case of yearly or longer study periods (**II**, **III**), only the data (of sap flow and environmental variables) within the growing season were used. Growing season was defined at the fifth consecutive day with daily mean $T \geq 5$℃ (**II**) or the first day with $S \geq 0$ ℃ (Eq. 16) (**III**). The difference between the two definitions was small (< 10 days).

Stem radial dimension

Point dendrometer with 1-µm accuracy (AX-5, Solartron Metrology, UK) was installed on each sample tree at breast height (**III**). The outer bark at the measurement locations was removed prior to the installation, and the sensors were installed against the inner bark (i.e. phloem). At Ränskälänkorpi, each dendrometer was installed through a plate, which was attached to the tree using metal rods penetrating into the heartwood. Both the plates and the rods were made of Invar (FeNi36 alloy) known for near-zero thermal expansion. At Hyytiälä, the dendrometers were

Table 3 Information on the estimated parameters of the whole-tree LOSM. See *Symbols* for their definitions and typical units. First use refers to the first equation in the main text in which the parameter is used while the dash sign (–) denotes those not presented. In Specificity, AG, Tr, and – denote age-group-, tree-, and non-specific (i.e. one value for all sample trees) parameters, respectively.

Parameter	First use	Specificity	Study	Reference of prior range
λ	Eq. 6	AG	**I**	Hari and Mäkelä (2003)
ι	Eq. 12	AG	**I**	ibid.
γ	Eq. 12	AG	**I**	Markkanen et al. (2001) Mäkelä et al. (2004) Kolari et al. (2014)
		–	**II, III**	**I**
ρ_{lw}	Eq. 28	Tr	**I**	Vanninen et al. (1996) McDowell et al. (2002)
χ	–	Tr	**I**	Phillips et al. (1997)
β	–[a]	–	**III**	**I**
ξ_m	Eq. 31	Tr	**II**	Päivänen (1973) Duursma et al. (2008) Nikinmaa et al. (2013)
		Tr, year	**III**	
ξ_p	Eq. 31	–	**II, III**	ibid.
η_m	Eq. 32	–	**II**	ibid.
		Tr	**III**	
η_p	Eq. 32	–	**II, III**	Moldrup et al. (1997)
d^*	Eq. 32[b]	–	**II, III**	Hökkä et al. (2021)
z_0	Eq. 25	–	**III**	Hari and Mäkelä (2003) Hölttä et al. (2017)
		year	**III**	**I**
z_1	Eq. 25	–	**II**	ibid.
		year	**III**	
c	Eq. 15	Tr	**II**	Mäkelä et al. (2004)
		Tr, year	**III**	

[a] Based on a finding of **I** on the linear correlation between χ and tree height (h), $\beta = \chi/h$, instead of χ itself, was an estimated parameter in **III**.
[b] After being converted to the optimal SWC (θ^*) using Eq. 51.

installed with rectangular steel frames (see Mencuccini et al. [2013] for illustration). Thus, they recorded DBH dynamics, and the data correction against frames' thermal expansion/contraction was conducted following Sevanto et al. (2005). The location of each dendrometer was changed before the beginning of each growing season at Hyytiälä. Only the data during growing seasons

were used. The intervals between the onsets of growing season and l_{BH} growth (132nd day of the year [DOY]; Jyske et al 2014) ranged 20—40 days, which were in accordance with theoretical estimate related to hormone transport and regulation (Vaganov et al. 2006). The temporal resolution of data was 30 min.

Model parameterization and performance assessment

To reflect tree age/size-related effects in the whole-tree LOSM, approximately a half of the estimated parameters were set tree- or age-group-specific, i.e. the estimate differed for each tree or age group, with prior ranges based on literature (Tables 3 and 4). The MAP estimates of the parameters were sought by adaptive MCMC algorithm DREAM$_{(ZS)}$ (Vrugt et al. 2009) in R (R Core Team 2019, 2020, 2022) with package 'BayesianTools' (Hartig et al. 2019).

To assess the performance of FM, linear regression was conducted between observed and modelled (using the parameters' MAP estimates) target variables, which are sap flow density (**I**) or transpiration rate (**II**, **III**) and SRD (**III**). Root-mean-square error (RMSE) was also calculated for assessing model performance, which is defined as

$$\mathrm{RMSE} = \sqrt{\frac{\sum_n(\boldsymbol{\varepsilon} \cdot \boldsymbol{\varepsilon})}{n}} \tag{52}$$

where n is the total number of elements in $\boldsymbol{\varepsilon}$.

Table 4 Information on the estimated parameters of the SRD model. See *Symbols* for their definitions and typical units. See Table 3 for the explanations of the columns except for "Study" as SRD was modelled only in **III**.

Parameter	First use	Specificity	Reference of prior range
ε	Eq. 35	Tr, year	Nobel (2020)
$\psi_{\phi 0}$	Eq. 46	–	Cabon et al (2020)
T_0	Eq. 47	–	ibid.
ΔH_a	Eq. 47	–	Parent et al (2010)
ΔH_d	Eq. 47	–	ibid.
ΔS_d	Eq. 47	–	ibid.
m	Eq. 48	Tr, year	Estimated
τ_c	Eq. 48	Tr, year	Estimated
ϕ_{max}	Eq. 47	Tr, year	Cabon et al (2020)

RESULTS

Model performance

The performance of the whole-tree LOSM was generally good regarding observed-to-modelled fitted slope (FS) of output variables (*E* and SRD) as well as R^2 (Table 5). Nevertheless, there were notable differences in RMSE between versions. The simplest version (without belowground module; **I**) showed the largest of all cases RMSE = 424.8 µmol m^{-2} leaf s^{-1}. However, note that this RMSE of *E* was converted from RMSE of *J*, 1.85 mol m^{-2} sapwood s^{-1}, by dividing the mean of tree-specific $\hat{\rho}_{\mathrm{lw}}$. With the belowground model structure (excluding waterlogging effects) and without parameterizing ρ_{lw}, RMSE was reduced to approximately only a fifth (79.41 µmol m^{-2} leaf s^{-1}; **III**) of that in **I** on a similar site at Hyytiälä. For the drained peatland sites at Sattasuo (**II**) and Ränskälänkorpi (**III**), the model with waterlogging effects resulted in similar (81.35 µmol m^{-2} leaf s^{-1}) or yet lower RMSE (60.10 µmol m^{-2} leaf s^{-1}). The model performance on SRD was also good, presenting fitted slope of observed to modelled values and R^2 close to 1 and RMSE < 90 µm (Table 5).

Hydraulic conductance and marginal water use efficiency (MWUE)

The above-ground model (**I**) showed that modelled stomatal conductance (g_σ) using $\hat{\lambda}$, $\hat{\iota}$ and $\hat{\gamma}$ (Table 3, Eq. 11 and 12) was almost always higher in younger/shorter than in older/taller Scots pine trees (Figure 3). Exceptions occurred under the condition that both *D* and *I* were close to the measured maxima, but in that case the difference in g_σ was small (< 0.1 mm s^{-1}). With the belowground model and waterlogging effects (**II**, **III**), modelled mean k_{sr} (per sapwood area) of Norway spruce was higher than that of Scots pine, and k_{sr} reduction (waterlogging effect) occurred

Table 5 Model performance on transpiration rate (*E*) and stem radial dimension (SRD). RMSE (root-mean-square error) are in µmol m^{-2} leaf s^{-1} for *E* and µm for SRD. FS, fitted slope of observed (*y*) to modelled (*x*) values; Rkp and Hyy (**III**), sites Ränskälänkorpi and Hyytiälä, respectively. $P < 0.0001$ for all FS.

			III			
	I *(E)*	**II** *(E)*	*E*		SRD	
			Rkp	Hyy	Rkp	Hyy
FS	1.013	0.991	0.916	0.939	1.000	0.973
R^2	0.755	0.801	0.763	0.860	0.996	0.980
RMSE	424.8	81.35	60.10	79.41	59.60	84.63

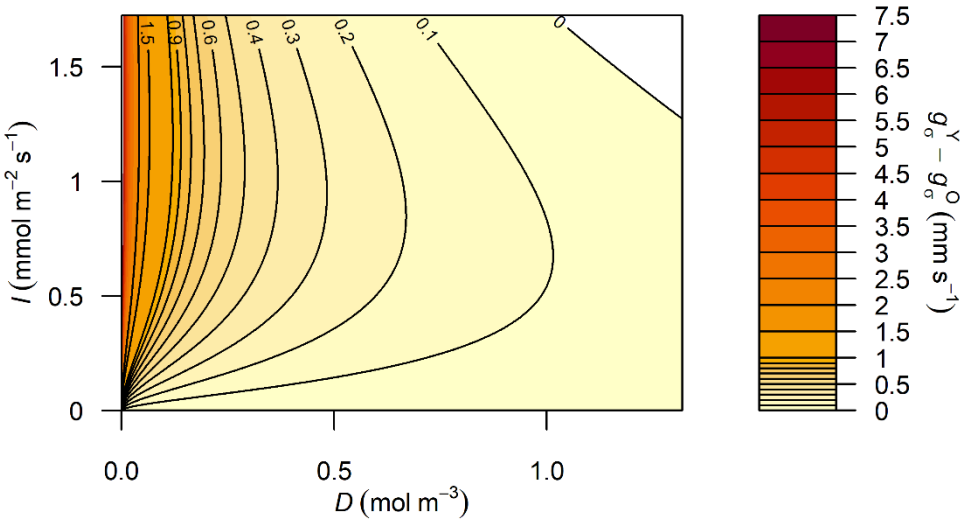

Figure 3 Modelled stomatal conductance difference between young and old *Pinus sylvestris* trees ($g_\sigma^{\mathrm{Y}} - g_\sigma^{\mathrm{O}}$) estimated using age-group-specific $\hat{\lambda}$, $\hat{\iota}$ and $\hat{\gamma}$ (Table 3, Eq. 11 and 12; **I**) in relation to *D* and *I* gradients. White area corresponds to negative values (top right), minimum = -9.54 × 10^{-2} mm s^{-1}.

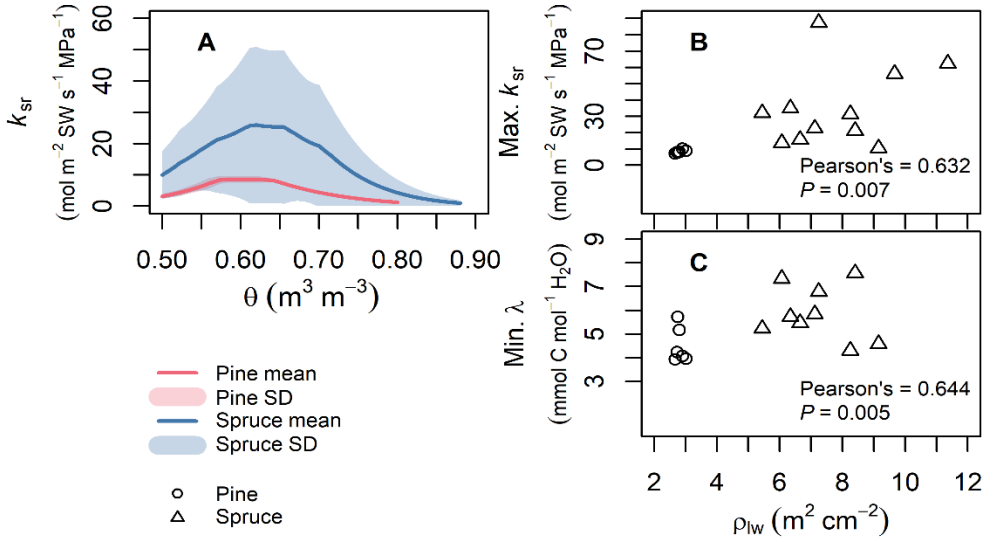

Figure 4 Modelled species-wise mean ± standard deviation (SD) soil-to-root conductance (k_{sr}, per sapwood [SW] area) of Scots pine (**II**) and Norway spruce (**III**) in relation to soil water content (θ; **A**), and maximum k_{sr} (**B**) and minimum marginal water use efficiency (λ; **C**) of individual trees in relation to leaf-to-sapwood area ratio (ρ_{lw}).

at slightly higher soil moisture (Figure 4A). Both the maximum k_{sr} and minimum λ were significantly correlated with ρ_{lw} (Figure 4B,C).

Cambial growth, phenology and assimilation

In contrast with the good performance of FM on SRD (Table 5, Figures 5 and 6), both AMs failed to capture the seasonal pattern of SRD at both sites. AM1 (without growth phenology expressed by the Gompertz function) produced SRD chrono-sequence noticeably more linear than the observations, and thus in most cases AM1 underestimated SRD in early growing season while overestimated later (with few exceptions e.g. Pentti 2019 at Hyytiälä; Figure 6). Failed in the temporal pattern before the yearly maximum SRD, AM2 (using only the Gompertz function to simulate growth) generated sigmoid curves with a too steep increase for the trees at Ränskälänkorpi (Figure 5). For Hyytiälä, AM2 overestimated SRD during early growing seasons of regular years (e.g. Pentti 2017, Figure 6) but late seasons of drought years (e.g. Sylvi 2019, Figure 6).

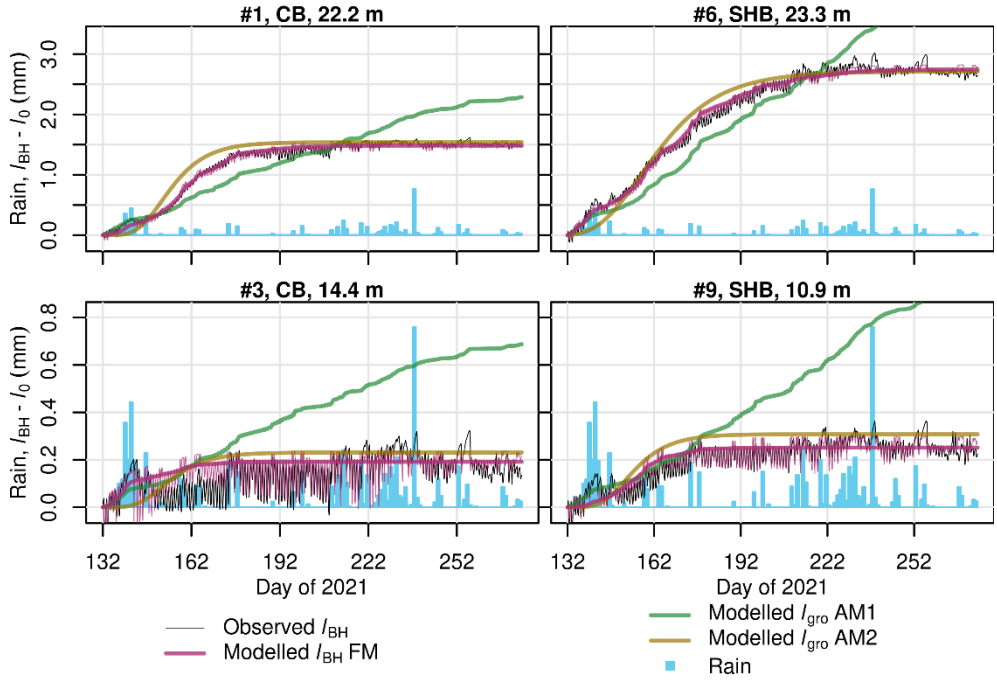

Figure 5 Stem radial dimension (l_{BH}) difference from the initial value of the year (l_0) of the Norway spruce trees at Ränskälänkorpi. For clarity, only four selected trees are displayed, and the hydraulic component (l_{ela}, cf. l_{gro}) of l_{BH} simulated by the alternative models (AMs) is omitted. In AM1 $N_c^{(AM1)} \equiv N_c^{max}$ in Eq. 45, and in AM2 Eq. 46 and 47 are unused and $\mathcal{g}^{(AM2)} \equiv \phi^{max} \cdot 1\ \mathrm{MPa}$ in Eq. 49. The title of each panel displays tree number and block, namely, control (CB) or selection harvest (SHB), and tree height.

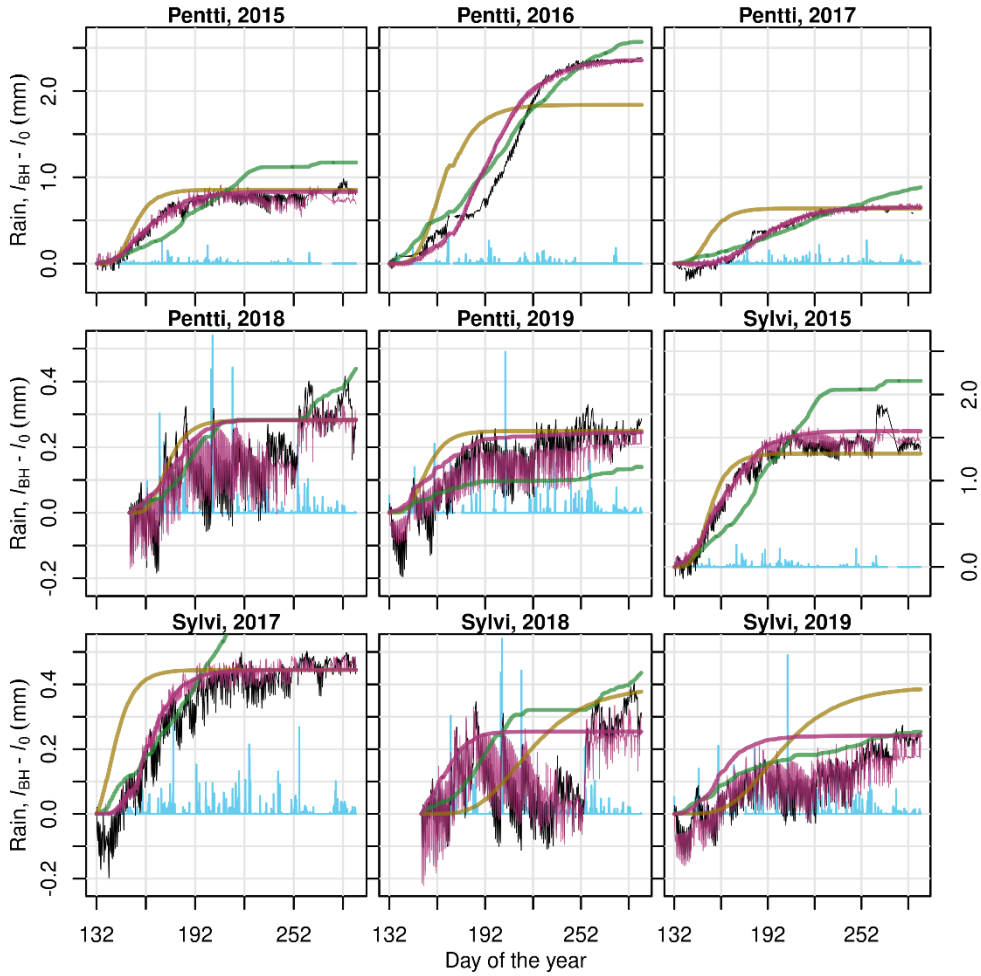

Figure 6 Stem radial dimension (l_{BH}) difference from the initial value of the year (l_0) of the Scots pine trees at Hyytiälä. The legend and the differences between FM and AMs in growth model structure are the same as in Figure 5. The title of each panel displays tree name and year.

Of all the correlation analyses of growth/phenological traits and leaf-specific photosynthetic production (P, i.e. A summed over time; mol C m^{-2} leaf), only growth duration vs growing-season production (P_{gs}) at Ränskälänkorpi was significant when an outlier was unused (Pearson's = 0.679, $P = 0.03$; Cook's distance of the outlier = 1.9 when used; Figure 7B). However, no such significant correlation was found at Hyytiälä, and P_{gs} there appeared to be of low variance with respect to growth duration. No significant correlations ($P > 0.1$) were found between timing of (t_{onset}) and production (P_{onset}) by cambial growth onset or between annual increment of basal area and P_{gs} (Figure 7A,C).

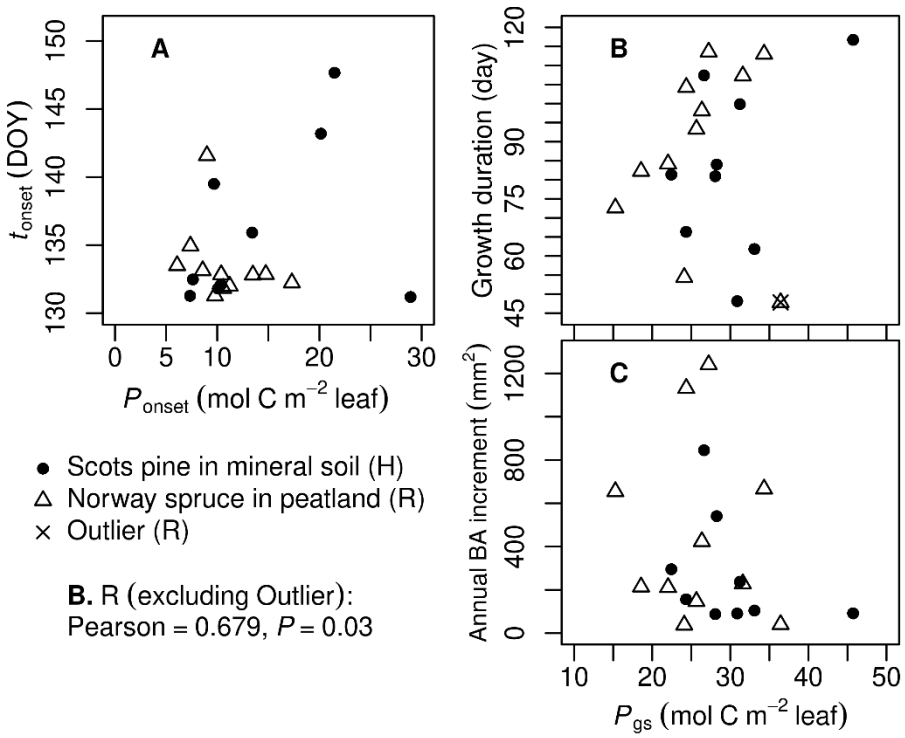

Figure 7 Growth and phenological traits in relation to photosynthetic production. The production was calculated by summing over the time period by cambial growth onset (P_{onset}; **A**) and over the whole growing season (P_{gs}; **B,C**), respectively. t_{onset}, timing of cambial growth onset; H and R, sites Hyytiälä and Ränskälänkorpi, respectively. All Pearson's correlation coefficient's $P > 0.1$ except for the one displayed on the bottom left. BA, basal area (**C**).

DISCUSSION

Model performance, structure and parameterization

To expand LOSM to whole-tree applications, the current study employed statistical (Bayesian) tools and/or mechanistic analyses to address aboveground and belowground water transport (**I**, **II**) and finally coupled the expanded LOSM with a cambial growth model focussed on sink activities and growth phenology (**III**). During its development, the model was used for investigating tree age/size-related effects on stomatal and soil-to-root conductances, marginal water use efficiency, and the correlation between cambial phenology and photosynthetic production. The good model performance suggests that the aims of model development were obtained in the planned stepwise manner. Compared with the statistical and simplistic version (**I**), incorporating semi-mechanistic formulation of belowground hydraulics (including waterlogging effects) in **II** reduced the model

error in simulating E considerably. This improvement supports the necessity of accounting for mechanisms of water uptake and whole-tree transport on the yearly scale. Furthermore, the coupled model (**III**) performed well on both hydraulics and SRD dynamics at a finer temporal resolution (30 min vs 1 day in **II**), and the error of E is lower than or similar to that in **II**. Therefore, the model was improved between versions corresponding to the respective aims.

The simulation of E presented a higher RMSE but also higher R^2 for Hyytiälä than for Ränskälänkorpi (RMSE = 82.29 vs 56.77, R^2 = 0.903 vs 0.785). The current design of tree-year-specific parameters for Hyytiälä (Tables 3 and 4) should have captured the *interannual* variances of E (J) and its direct environmental factors (D and I). Thus, the RMSE and R^2 results are likely related to the *intra-annual* variances of the variables during the growing season at Ränskälänkorpi, which is reflected by the higher coefficient of variation (CV) of D and I. At Ränskälänkorpi, CV_D = 1.09 and CV_I = 1.26, higher than at Hyytiälä (CV_D < 1.07, CV_I < 1.26). Another source of structural error for Ränskälänkorpi may be the variance between trees in non-stomatal limitations on photosynthesis (parameters z_0 and z_1). As there was only one estimate for each of them for the site, this between-tree variance may not be well represented in the model and may have heavily influenced the likelihood output of the model (Figure 8). This design was due to the difficulty in quantifying the between-tree variances of the factors of z_0 and z_1 (e.g. the maximum carboxylation capacity without non-stomatal limitation; Eq. 22—25, Figure 1). The difference in model performance on E between sites may also be related to the difference methods of measuring sap flow (heat pulse vs thermal dissipation). The heat pulse method employed at Ränskälänkorpi has been known of higher sensitivity and accuracy than the thermal dissipation method at Hyytiälä (Steppe et al. 2010). Consequently, less variation of sap flow was recorded at Hyytiälä (CV_J = 1.32, all data combined) than at Ränskälänkorpi (CV_J = 1.42, all data combined).

The full model's (FM) performance on SRD was good for both Hyytiälä and Ränskälänkorpi. However, the worse performance under drier conditions (Hyytiälä than Ränskälänkorpi, especially in dry years 2018 and 2019) is noteworthy, particularly regarding the SRD expansion and contraction associated with rain events (e.g. Sylvi 2018 in Figure 6). There are three possible reasons behind this phenomenon, namely, bark hydraulics formulation related to rain events, MOE being constant to water potential, and constant osmotic potential (i.e. its absence from Eq. 43). Currently, bark hydraulics (Eq. 40—42) is formulated simplistically for lacking direct quantitative experimental support. Particularly, its water inlet (Eq. 41) seems to have been underestimated regarding the underestimated SRD expansion following rains. However, a more realistic model would incur considerable complexity of, for example, stem flow dynamics, which were beyond the scope of the current model. Variable MOE is suggested by the heteroscedastic daily SRD fluctuations between two rain events in dry years at Hyytiälä. The dry wood should have had lower MOE than the current time-invariant estimates, which is in accordance with previous results of dehydration-rehydration experiments on sawn logs (e.g. Tyree and Yang 1990; Tyree and Zimmermann 2002). Also, the dependence of MOE on water potential has been hypothesized (e.g. De Scheppe and Steppe 2010). Nevertheless, implementing such dependence into the current model yet requires more precise prior knowledge on live trees for calibrating new parameters that it would introduce.

Although osmolality at stem base of boreal conifers is of low variance through the growing season (Paljakka et al. 2017), its dynamics missing from estimating ψ^{cam} (Eq. 43) may have entailed errors in the current simulation of $\dot{I}_{\mathrm{ela}}$ under occasional droughts with rain events. The higher errors associated with rain events at Hyytiälä suggest that $\dot{\psi}_{\mathrm{BH}}$ was underestimated (or MOE overestimated as already discussed). The Höfler diagram has shown that osmotic potential (ψ_{Π}) decreases simultaneously with hydrostatic potential as dehydration occurs but with a slope lower

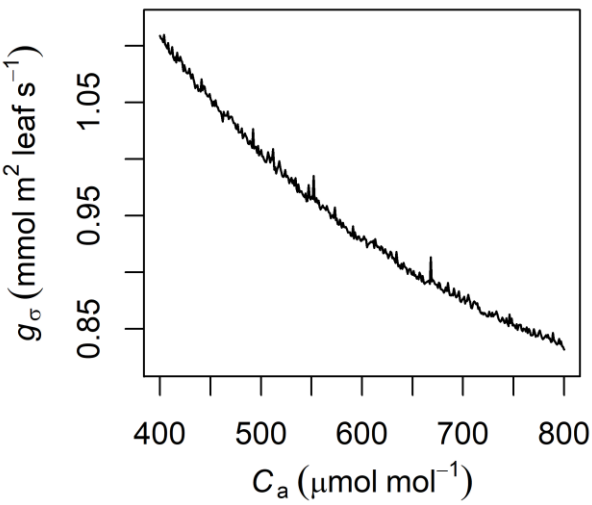

Figure 8 Predicted mean stomatal conductance (g_σ) with increasing atmospheric CO_2 concentration ($\mathcal{C}_a$) using Eq. 13—15, 23 and 24. The mean was calculated from the joint variation of g_σ with variables $D \in$ (0, 1.3] (mol m^{-3}), $I \in$ (0, 1.3] (mol m^{-2} s^{-1}), $T_l \in$ [-5, 33] (°C), $S \in$ [0, 23] (°C), $k_{sl} \in$ [2, 300] (mmol m^{-2} s^{-1} MPa^{-1}) (all within their respective measured or modelled ranges in **III**), and $\mathcal{C}_i/\mathcal{C}_a \in$ [0.5,0.7]. The variables were assumed independent from each other. Means of $\hat{c}$ and $\hat{\gamma}$ in **III** were used, and the other parameters ($\mathcal{V}_c^{max}$, $\mathcal{M}$, Γ^* and ψ_{A0}) had the same values as for Figure 1.

than the latter (Jones 2014; Nobel 2020). Thus, accounting for $\dot{\psi}_\Pi$ in Eq. 43 should improve the model performance on $\dot{l}_{ela}$ and thus SRD under rains. Ideally ψ_Π is approximately the product of the ideal gas constant, temperature, and the summed concentrations of osmotically active solutes ($\sum_j[X_j]$), whereas in reality the slope $\psi_\Pi/\sum_j[X_j]$ does not hold constant for some compounds (e.g. sucrose) when the concentrations are low due to dissociation (Nobel 2020). Therefore, calibrating $\psi_\Pi(\sum_j[X_j])$ and implementing it into the current model should require sampling and chemical assay of the sap over a wide gradient of concentration as an additional input of the model. An alternative and easier practice is using the osmometer to obtain a chrono-sequence of osmotic water potential. However, neither of the methods was conducted in the current study.

Upon analysing similar formulation of non-stomatal limitations on photosynthesis, Dewar et al. (2018) have drawn the conclusion that the Cowan-Farquhar type of LOSM predicts wrong stomatal response to increasing $\mathcal{C}_a$ when λ is constant, which is directly related to the goal function of optimization (Eq. 5). In the current model, λ is variable and a function of k_{sl}, with which g_σ (Eq. 13—15, 23 and 24) is predicted to have a long-term decreasing trend with increasing $\mathcal{C}_a$ (Figure 9), reduced by *c*. 25% under doubled $\mathcal{C}_a$ (800 ppm vs 400 ppm). This predicted reduction is close to the mean decrease of stomatal conductance (19% for trees and 21.7% for all the studied C_3 plants) observed in free-air CO_2 enrichment (FACE) experiments (Ainsworth and Rogers 2007). Thus, the current model improved the g_σ response to increasing $\mathcal{C}_a$ compared to the basic LOSM.

However, the interactions between physiological parameters and environmental factors, e.g. increased Γ^* and $\mathcal{M}$ under increasing temperature (Galmés et al. 2016; Busch and Sage 2017), were not addressed in this prediction. New model calibration must be conducted for a more holistic perspective of $g_\sigma(\mathcal{C}_a)$ with such interactions included, and the increases of Γ^* and $\mathcal{M}$ are expected to influence the numerical approximation (Eq. 25) as they are lumped into the empirical coefficients z_0 and z_1. Therefore, such variations in photosynthetic traits will affect $\lambda(k_{sl})$ within the current model structure, which needs to be confirmed by more specific observations on the interactions of plant water use, hydraulic conductance and changing environment.

Physiological effects related to tree age/size and structure

The model predicted higher stomatal conductance of young/short than old/tall trees (Figure 3) and that k_{sr} and λ were positively correlated with ρ_{lw} (Figure 4). The decline of stomatal conductance with increasing tree size/age has been reported widely (e.g. Niinemets 2002; Koch et al. 2004; Ryan et al. 2006; Steppe et al. 2011; Tor-ngern et al. 2017), which is a typical adaptation to increased hydraulic resistance against transporting water to higher foliage. This decline may further contribute to the decreased assimilation rate (per leaf area and mass) in high foliage (Niinemets 2002) and the growth of old trees (especially height growth; Koch et al. 2004; Ryan et al. 2006; Martínez-Vilalta et al. 2009). According to the basic LOSM (Eq. 10 and 11) and its parameterization used for this prediction, young trees had higher $\hat{\imath}$ and thus faster increase in g_σ in comparison to old trees when I was increasing at low to medium levels (**I**). However, young trees became more sensitive to D than to I at relatively low levels of the factors according to the analyses of $\partial g_\sigma/\partial D$ and $\partial g_\sigma/\partial I$ (**I**). Consequently, they were more strongly affected by dryness than the old trees, which resulted in the negative $(g_\sigma^{\mathrm{Y}} - g_\sigma^{\mathrm{O}})$ at high D and I. These results are likely related to the larger water storage in the old/larger trees, while k_{sr} of large trees may have also contributed to their stronger drought-tolerance (Figure 4A,B; Scholz et al. 2011).

The higher k_{sl} (per *sapwood* area) of Norway spruce than Scots pine in moist soil (Figure 4A) is related to spruce's higher ρ_{lw} (Figure 4B) and higher tolerance to waterlogging. As unit sapwood area of Norway spruce hydraulically supports a larger area of foliage, it needs a higher efficiency of water uptake at roots than Scots pine's. The higher k_{sl} of spruce may be realized by morphological adaptations of fine roots, including higher mean dry mass, length and volume of root tips (Ostonen et al. 2007). Additionally, Norway spruce has the plate root system, featuring massive lateral roots spreading horizontally in shallow soil, in contrast to the tap root system of Scots pine featured with a noticeably dominant coarse root growing vertically into deep soil. This structural feature of Norway spruce facilitates its water uptake (k_{sr} of the whole root system) from shallow soil under favourable SWC as well as waterlogging-tolerance when WTD is not extremely high. However, the site-related effects (Scots pine from Northern Finland in **II** vs Norway spruce from southern Finland in **III**) on this inter-specific comparison are yet to be clarified. For instance, both species have higher shallow-soil (humus and mineral soil with depths < 10 cm) fine root density (dry mass per soil volume) in northern than in southern Finland (Helmisaari et al. 2007). Also, nutrient conditions were not accounted for in this cross-site comparison, which has long been known to affect rhizosphere as well as whole-tree structure (e.g. Vogt et al. 1995; Vanninen and Mäkelä 1999; Leuschner et al. 2004; Jager et al. 2015; Kramer-Walter et al. 2016). Such site-related effects may be considerable when comparing root-related attributes across a great geographical difference.

The increasing λ with increasing ρ_{lw} (Figure 4C) and tree size is in accordance with the earlier findings of higher ^{13}C fractionation ($\delta^{13}C$) and thus higher water use efficiency (WUE) in the top foliage of taller trees (Koch et al. 2004; McDowell et al. 2011; Brienen et al. 2017), if λ (*marginal* WUE) is interpreted as WUE at an infinitesimal time step. This increase in WUE with increasing tree height is another adaptation to higher risk of local drought in higher foliage, additional to the lower g_σ of old/tall trees reflected in Figure 3. That minimum λ of spruce showed less variance than maximum k_{sr} over the same range of ρ_{lw} may suggest that the limiting factor of k_{sl} changes correspondingly to SWC, being k_{sr} under dry or waterlogging conditions (i.e. $k_{\mathrm{sr}} \ll k_{\mathrm{rl}}$) but k_{rl} under favourable SWC (i.e. $k_{\mathrm{sr}} \gg k_{\mathrm{rl}}$). It is clear from Eq. 27 that whichever of k_{sr} and k_{rl} that is much smaller than the other determines the scale of k_{sl}. Therefore, k_{sl} and λ appear to be stabler

than k_{sr} across SWC gradient upon the tree-wise constant k_{rl} in the current model (Eq. 28), which in turn stems from the comparatively constant maxima J (and thus E) and $|\psi_s - \psi_l|$ when the sensitive stomata start to close and restrain water loss.

Cambial growth in relation to carbon gain and sink activities

In recent years, tree growth modelling has been developing towards a balance between carbon source and sink activities in contrast to photosynthesis-centred formulation previously (see *Introduction – Modelling tree stem radial growth*). Converse to such earlier formulation, the prototype of the current model (Johnson et al. 1942; Parent et al. 2010; Cabon et al. 2020) describes solely the sink activities of the cambium and thus was expected to provide a novel structure for sink-driven growth modelling. Despite the successful tests on a variety of temperate crops and trees (Parent and Tardieu 2012), the prototypical model failed to capture the seasonal pattern of the current boreal trees' cambial growth (Figures 5 and 6), and the failure of both alternative models (AMs) suggest that empirical (phenological) part of the growth model is as indispensable as the mechanistic (biophysical) one. The Gompertz function has been found good at predicting the number of enlarging cells decaying through the growing season, which may be related to the shorter time that cambial cells stay in enlargement in late growing season (Cuny et al. 2013). Thus, without representing phenology, AM1 essentially assumes a constant N_c through the growing season, a hypothesis rejected decades ago (e.g. Wodzicki 1971). This asymmetrical temporal pattern may be a synergy of carbon availability and other factors e.g. hormonal control. The present analyses show that growing-season photosynthetic production (P_{gs}) was correlated with length of growth duration at the moister site (Ränskälänkorpi; Figure 7B), which may be related to carbon shortage in late growing season as boreal conifers under limited carbon gain tend to store carbon rather than allocate it to growth (Huang et al. 2021). In contrast, growth onset (Figure 7A) likely depends on hormone spreading instead of carbon availability (Vaganov et al. 2006; Hartmann et al. 2021). Consequently, the annual area increment of wood was not correlated with photosynthetic production (Figure 7C), which is in accordance with the earlier finding of the pivotal role of phenological control in woody growth and its decoupling from carbon gain (Delpierre et al. 2016b). Therefore, evidence is yet insufficient for equalling growth phenology and effects of carbon source activities, and phenology per se should be accounted in tree growth modelling.

It should be noted that the growths of other tree compartments (e.g. foliage) or traits (e.g. height) may differ from that of the cambium. Thus, the current model should be integrated with, for example, carbon balance analysis to account for carbon allocation and to draw a holistic conclusion on source and sink limitations on whole-tree growth. Also, modelling carbon allocation to storage is necessary for a better prediction of tree growth on larger temporal scales. The storage dynamics should include, at least, those of short-term use (sugars) and longer-term storage (e.g. starch) as they function distinctly for tree physiology. Such detailed modelling of carbon storages should also help clarify the physiological connection between phenology and carbon gain (Figure 7D,E), as NSC is critical for plants to recover from winter and start growth in spring (Linkosalo et al. 2006; Hartmann and Trumbore 2016; D'Andrea et al. 2021). This enhancement may be realized by coupling the current model with an existing model focussed on carbon allocation and storage (e.g. CASSIA, Schiestl-Aalto et al., 2015), and the parameterization methods based on Bayesian inference and MCMC algorithm should be similar to those employed in the current study. However, at least two major difficulties must be tackled firstly, namely, 1) measured reference for

quantifying dynamics of sugars and starch and 2) unifying the temporal resolution of the modelled carbon source and sink activities.

Future research

Additional to the potential improvements and enhancements discussed in the previous sections, new eco-physiological objectives and mathematical tools should be considered in future research based on the present works, including but not limited to the examples as follows.

Firstly, phloem functionality (e.g. processes of assimilate transport and osmoregulation) should be integrated into the model for a holistic view of the vasculature. As hypothesized and tested for decades (Münch 1930; Gould et al. 2005; Lambers et al. 2008; De Schepper et al. 2013; Knoblauch et al. 2016), the water transport in the xylem and the sugar transport in the phloem are functionally inseparable through osmotic dynamics. This future work may be a further development from the carbon storage modelling discussed in the previous section, and pioneering works have been available (e.g. Hölttä et al. 2017; Perri et al. 2019; Schiestl-Aalto et al. 2021). Another key factor of growth is hormonal control, and it needs corroboration in process-based and physiology-orientated growth models as well. Theoretically and ideally, growth-related hormones spread following Fick's law of diffusion, and thus the hormone concentration ([X]) at a position of interest (x) can be approximated by (Hartmann et al. 2021)

$$[\mathrm{X}](x) = [\mathrm{X}](0)\exp\left(-\frac{x}{\omega}\right) \tag{53}$$

(ω, a coefficient), which is algebraically similar to the derivative of Gompertz function (Eq. 48). This algebraic resemblance is because of the exponential decay in both processes. It may be the mathematical reason behind the good fitting of Gompertz function to the dynamics of cambial growth. Despite this idealistic analysis, the composition, functionality and dynamics of hormones related to cambial growth (reviewed by Sorce et al. [2013]) are yet to be experimentally scrutinized and mathematically described in a modelling framework with appropriate complexity.

The current expression of the time lag between transpiration and sap flow dynamics does not explain related mechanisms and may have limited model performance on SRD. To improve, water storage properties (e.g. hydraulic capacitance) may be introduced into the framework. System identification tools (e.g. transfer function and state-space analysis) may help in this aspect, which have been widely applied in electrical control engineering (e.g. Ogata 2010). Transfer function is the ratio of a system's complex output to input, transformed using the Laplace transform or the *Z*-transform. It has been used for estimating the time constant of simplified whole-tree hydraulic system (Phillips et al. 1997; Phillips et al. 2004). The simplification is mainly due to the applicability of transfer function that is, strictly speaking, limited to linear systems. On the contrary, real tree vasculature often presents notable features of the non-linear and time-variant system, for example, embolism, variable MOE dependent on water content/potential, and variable capacitance due to the non-linear variable ψ_Π (see *Discussion – Model performance, structure and parameterization*). With this respect, state-space analysis is more versatile as empirical expressions of the time-variant properties can be embedded into the state matrix, and tools for estimating coefficients in the state space have been available (e.g. Young 2000; Young et al. 2001; Taylor et al. 2007). Despite the powerful potential of these tools for system identification, the analogy of tree hydraulics to electrical network is obscure in detail (e.g. the physiological definition of

'capacitor' and how parts are connected). Also, testing the hypothetical model requires extremely demanding measurements (especially of water potential), and the presentation of the complex analyses is challenging.

Additionally, the waterlogging effects need to be modelled more mechanistically. Its current formula ($k_{\mathrm{sr}}^{-}(\theta)$, Eq. 32) algebraically mirrors $k_{\mathrm{sr}}^{+}(\theta)$ without waterlogging effects (Eq. 31) based on the qualitative observation comparing flooding, drought treatments and control (Domec et al. 2021). This model design does account for the spare soil porosity ($1-\theta/\theta_{\mathrm{sat}}$) but not specifically the oxygen content, whereas anaerobic respiration (fermentation) under hypoxia/anoxia is one of the direct causes of impaired plant functioning (Kreuwieser and Rennenberg 2014). Fermentation inhibits root functioning by generating less adenosine triphosphate (ATP) per used glucose (*c.* one twentieth of aerobic respiration) and accumulating hazardous by-products (e.g. alcohol) (Ferner et al. 2012). These phenomena increase the sugar demand (i.e. sink strength) of roots, and thus maintaining normal photosynthesis rate and transporting assimilates to roots under waterlogging stress is the most important feature of flood tolerance (Ferner et al. 2012; Kreuwieser and Rennenberg 2014). Therefore, from a modelling perspective, waterlogging effects may be regarded as feedback to photosynthesis and phloem transport in future models, albeit little is certain yet in understanding the exact physiological reasons of reduced root hydraulic conductance (e.g. aquaporin expression) or root-to-shoot signalling under the impairment (Kreuwieser and Rennenberg 2014).

The coupled model in the current study may contribute to incorporating the sink pathway of environmental growth control into the larger-scale dynamic vegetation model (DVM). DVMs describe vegetation and soil processes, predict changes in their structure and distribution, and are commonly centralized around photosynthesis and carbon fluxes (Friend et al. 2019). Similar to the aforementioned challenge to the photosynthesis-driven growth models (*Introduction – Modelling tree stem radial growth*), the central role of carbon processes in DVMs has also been shaken due to the considerable uncertainties in their future prediction under changing climates (Friedlingstein et al. 2014). Therefore, calls for including sink activities in DVMs have been widely made, and introducing a xylogenesis model balanced between carbon processes and sink control can be an important improvement in this regard (Zuidema et al. 2018; Friend et al. 2019; Eckes-Shephard et al. 2022; Friend et al. 2022). The current model may act a role in this improvement provided that explicit formulation of carbon storage and phloem functioning is implemented as discussed earlier. Yet, upscaling from the current scale of individual tree to ecosystem is challenging due to, for instance, the variances of the individuals' physiological traits and the corresponding parameter design. Also, calibrating the upscaled model using eddy covariance observations should be performed with caution, as disaggregating observed evapotranspiration to transpiration is scale-sensitive and yet to be adequately addressed (Knauer et al. 2018; Perez-Priego et al. 2018).

SUMMARY

Mathematical models of tree eco-physiology and growth have been developing for a long time, and their coupling is important for understanding trees' functioning and its responses to the changing environment. A key nexus between physiological and growth processes is stomata, which control the efflux of water and influx of carbon, the most important resources of plants. Modelling stomatal behaviour is based on the analysis of gas exchange at the aperture and its environmental factors, namely, temperature, water vapour pressure deficit (VPD), atmospheric CO_2 concentration, and photosynthetic photon flux density (PPFD). The stomatal optimality model employing functional analysis of gas fluxes is one of the most tested models of stomatal behaviour, where the optimality is defined to obtain maximum difference between summed carbon gain and summed water loss over a given time. The model can be expanded to describe whole-tree-level hydraulic processes, including water uptake and transport corresponding to stomatal control, and thus provide water potential at a place of interest (e.g. cambium at breast height) as a key input to a growth model. Such a growth model, therefore, can reflect the carbon sink activities during growth accounting direct effects of hydraulic factors. This contrasts with modelling environmental effects on growth indirectly through carbon gain (photosynthesis), which is a common but disputable practice in earlier large-scale forest growth models.

The stomatal optimality model aims at maximizing assimilation with a constraint of transpiration over a certain time. The solution of optimal stomatal conductance contains atmospheric CO_2 concentration, VPD (with temperature effect), PPFD reaction curve, and the Lagrange multiplier, and thus the model is termed Lagrangian optimal stomata model (LOSM) in the current study. The Lagrange multiplier can be interpreted as the marginal water use efficiency (MWUE) and correlated with soil-to-leaf conductance in an empirical log-log linear form. This simple correlation is a numerical approximation of a mechanistic analysis of non-stomatal limitations on photosynthesis, which accounts for photorespiratory compensation, carboxylation capacity (impacted by water potential), and the Michaelis-Menten kinetics of CO_2. The soil-to-leaf conductance can be broken down to two components i.e. soil-to-root and root-to-leaf conductances. In the studied coniferous species (Scots pine and Norway spruce), the relatively constant root-to-leaf conductance can be estimated using maxima sap flow density and water potential difference between soil and leaf. Soil-to-leaf conductance in typical mineral soils is a monotonically increasing function of soil water content (SWC) relative to its saturation level, whereas decline of conductance occurs when SWC is too high and roots are waterlogged. Quantitative observation of this decline is yet lacking, but qualitatively the decreased soil-to-root conductance under flooding is similar to that under drought. Hereby, LOSM is expanded to whole-tree application by correlating hydraulic conductances and MWUE and with waterlogging effects accounted for the trees in peatland.

The dynamics of stem radial dimension (SRD) have two components, namely, those caused by water storage dynamics (reversible, usually on the daily scale) and growth (irreversible, on larger temporal scales). Both components depend on water potential at the place of interest (breast height in the current study), which can be estimated using the whole-tree LOSM. Rainwater input can also be accounted for although highly simplified. The growth model was based on an analysis of enzymatic activation of cambial cells, which had been tested only on temperate plants. A phenological module was added in the current study, lest accounting only instantaneous effects on growth fail to capture season-scale environmental constraints. The model framework was tested against observed data in a stepwise manner: Test the whole-tree LOSM assuming the belowground

parts constantly optimal (**I**), including the belowground model structure (**II**), and test the coupled model of full whole-tree LOSM and SRD (**III**). The tests were associated with parameterization employing an adaptive Monte Carlo Markov chain (MCMC) algorithm.

The model performed well and became better from **I** to **III** on simulating transpiration rate. It showed that young/short Scots pine trees had higher stomatal conductance than did old/tall trees under the same PPFD and VPD except when both factors were very high. These results suggest the increased hydraulic resistance and storage in old/tall trees. The higher simulated soil-to-root conductance in Norway spruce than in Scots pine is in accordance with the positive correlation between maximum soil-to-root conductance and leaf-to-sapwood area ratio. Minimum MWUE was also positively correlated with leaf-to-sapwood area ratio but to a weaker degree, suggesting the limiting effect of root-to-leaf conductance under favourable SWC. The growth model describing only instantaneous cambial sink activities or using only empirical formulation failed to capture the seasonal pattern of SRD, suggesting that both the biophysical and phenological components of the growth model are crucial. Mean assimilation rate was correlated with cambial growth duration but not onset, and annual increment was not correlated with assimilation either. These correlations suggest that phenology is not fully determined by carbon source activities and should be included in growth models on itself.

The current model provides a good tool for predicting gas exchange at stomata and growth simultaneously at a fine temporal resolution (30 min). It also yields reasonable prediction of stomatal conductance responding to increased atmospheric CO_2 concentration. For the future, potential improvements are expected to address carbon storage and phloem functionality, to formulate the growths of other compartments of the tree, and to corroborate the physiological causes behind waterlogging effects. The model may also be used for improving larger-scale dynamic vegetation models, balancing between carbon processes and sink activities.

ACKNOWLEDGEMENTS

‘If I have seen further it is by standing on ye sholders [sic] of Giants,’ writes Isaac Newton (1959). Daring not claim a sight comparable to Sir Isaac's, however, so shall I say as well: I am cordially grateful to the great people who have shouldered me up so far. Had there not been their encouragement and support, I would not have realized this dream with so much delight.

My foremost thanks go to my primary supervisor, Professor Annikki Mäkelä, who manifested the art of modelling throughout these years since my first attendance of her courses. Her mathematical demonstration of physiological and silvicultural phenomena and processes has crucially helped me specify research direction and solidify my philosophy, while her open-mindedness let me explore a wide variety of subjects and methods in my own pace. In addition, the leading and supervision skills that I learnt from her shall benefit my future career profoundly, whatever it will be.

I present my gratitude to Professor Teemu Hölttä too, who is characterized by vivid new ideas as well as firm fundamental knowledge in tree eco-physiology, especially on the vasculature of trees. He was also open at almost any time to any talks in miscellaneous topics ranging from communicative issues with collaborators to fascinating development of tree physiology in the future. His guidance and support were irreplaceable for this degree.

The fieldwork, data and component articles of this doctoral study were facilitated by Professors Mikko Peltoniemi and Frank Berninger, Associate Professor Tuomas Aakala, Docent Yann Salmon, Drs Francesco Minunno, Tián Xiàng-Lín, Pavel Alekseychik and Hannu Hökkä, and staffs of Hyytiälä and Värriö researcher stations, especially Mr Janne Levula (now at Stora Enso), Dr Pauliina Schiestl-Aalto (Hyytiälä) and Mr Teuvo Hietajärvi (Värriö, retired). The practical issues in my course studies were solved with kind help of Dr Karen Sims-Huopaniemi, and this thesis was finalized with valuable comments from the preliminary examiners, Professor Belinda Medlyn and Dr Liisa Kulmala. I was financially supported by the ex-Doctoral School in Environmental, Food and Biological Sciences (YEB) of the University of Helsinki, the Finnish Society of Forest Science (SMS), and the Finnish Cultural Foundation (SKR), along with the Research Council of Finland (Suomen Akatemia) via my supervisors. I thank all these people and organizations.

My wellbeing through this long journey was enhanced by Timo and Eija’s film club, my department’s pikkujoulu, and the basketball and football games. I am grateful to the people who organized these activities and shared the joy with me therein. I thank my groupmates Francesco, Xiàng-Lín, Atte, Teemu (P), Jonathan, Joanna, Donggyu, Ismael, Ritika along with many other friends and colleagues (whose names, I regret, cannot be enumerated due to the limited space), for their company, ideas and tolerating my pedantry and redundancy in mathematics and speech. Finally, I feel deeply indebted to those who love or loved me for their patience, care and solitude.

25th July 2024
Helsinki, Finland

REFERENCES

Ainsworth EA, Rogers A (2007) The response of photosynthesis and stomatal conductance to rising [CO_2]: mechanisms and environmental interactions. Plant Cell Environ 30: 258-270. https://doi.org/10.1111/j.1365-3040.2007.01641.x

Ball JT, Woodrow IE, Berry JA (1987) A model predicting stomatal conductance and its contribution to the control of photosynthesis under different environmental conditions. In: Biggins J (ed) Progress in Photosynthesis Research, vol IV. Springer, Dordrecht, pp 221-224. https://doi.org/10.1007/978-94-017-0519-6_48

Beer C, Reichstein M, Tomelleri E, Ciais P, Jung M, Carvalhais N, Rödenbeck C, Arain MA, Baldocchi D, Bonan GB (2010) Terrestrial gross carbon dioxide uptake: global distribution and covariation with climate. Science 329: 834-838. https://doi.org/10.1126/science.1184984

Begum S, Nakaba S, Yamagishi Y, Oribe Y, Funada R (2013) Regulation of cambial activity in relation to environmental conditions: understanding the role of temperature in wood formation of trees. Physiol Plantarum 147: 46-54. https://doi.org/10.1111/j.1399-3054.2012.01663.x

Berdanier AB, Miniat CF, Clark JS (2016) Predictive models for radial sap flux variation in coniferous, diffuse-porous and ring-porous temperate trees. Tree Physiol 36: 932-941. https://doi.org/10.1093/treephys/tpw027

Bonan GB, Lawrence PJ, Oleson KW, Levis S, Jung M, Reichstein M, Lawrence DM, Swenson SC (2011) Improving canopy processes in the Community Land Model version 4 (CLM4) using global flux fields empirically inferred from FLUXNET data. J Geophys Res-Biogeo 116: G02014. https://doi.org/10.1029/2010JG001593

Bradshaw CJ, Sodhi NS, Peh KS-H, Brook BW (2007) Global evidence that deforestation amplifies flood risk and severity in the developing world. Global Change Biol 13: 2379-2395. https://doi.org/10.1111/j.1365-2486.2007.01446.x

Brienen R, Gloor E, Clerici S, Newton R, Arppe L, Boom A, Bottrell S, Callaghan M, Heaton T, Helama S, Helle G, Leng MJ, Mielikäinen K, Oinonen M, Timonen M (2017) Tree height strongly affects estimates of water-use efficiency responses to climate and CO_2 using isotopes. Nature Communications 8: article number 288. https://doi.org/10.1038/s41467-017-00225-z

Busch FA, Sage RF (2017) The sensitivity of photosynthesis to O2 and CO_2 concentration identifies strong Rubisco control above the thermal optimum. New Phytol 213: 1036-1051. https://doi.org/10.1111/nph.14258

Cabon A, Peters RL, Fonti P, Martínez-Vilalta J, De Cáceres M (2020) Temperature and water potential co-limit stem cambial activity along a steep elevational gradient. New Phytol 226: 1325-1340. https://doi.org/10.1111/nph.16456

Cabon A, Kannenberg SA, Arain A, Babst F, Baldocchi D, Belmecheri S, Delpierre N, Guerrieri R, Maxwell JT, McKenzie Sh, Meinzer FC, Moore DJP, Pappas Ch, Rocha AV, Szejner P, Ueyama M, Ulrich D, Vincke C, Voelker SL, Wei J-Sh, Woodruff D, Anderegg WR (2022) Cross-biome synthesis of source versus sink limits to tree growth. Science 376: 758-761. https://doi.org/10.1126/science.abm4875

Campbell GS (1974) A simple method for determining unsaturated conductivity from moisture retention data. Soil Sci 117: 311-314. https://doi.org/10.1097/00010694-197406000-00001

Chan T, Hölttä T, Berninger F, Mäkinen H, Nöjd P, Mencuccini M, Nikinmaa E (2016) Separating water-potential induced swelling and shrinking from measured radial stem variations reveals a cambial growth and osmotic concentration signal. Plant Cell Environ 39: 233-244. https://doi.org/10.1111/pce.12541

Clapp RB, Hornberger GM (1978) Empirical equations for some soil hydraulic properties. Water Resour Res 14: 601-604. https://doi.org/10.1029/WR014i004p00601

Clearwater MJ, Meinzer FC, Andrade JL, Goldstein G, Holbrook NM (1999) Potential errors in measurement of nonuniform sap flow using heat dissipation probes. Tree Physiol 19: 681-687. https://doi.org/10.1093/treephys/19.10.681

Collatz GJ, Ball JT, Grivet C, Berry JA (1991) Physiological and environmental regulation of stomatal conductance, photosynthesis and transpiration: a model that includes a laminar boundary layer. Agr Forest Meteorol 54: 107-136. https://doi.org/10.1016/0168-1923(91)90002-8

Cosby B, Hornberger G, Clapp R, Ginn T (1984) A statistical exploration of the relationships of soil moisture characteristics to the physical properties of soils. Water Resour Res 20: 682-690. https://doi.org/10.1029/WR020i006p00682

Cowan I (1982) Regulation of water use in relation to carbon gain in higher plants. In: Lange OL, Nobel PS, Osmond CB, Ziegler H (eds) Physiological Plant Ecology II. Springer, Berlin Heidelberg, pp 589-613. https://doi.org/10.1007/978-3-642-68150-9_18

Cowan IR, Farquhar GD (1977) Stomatal function in relation to leaf metabolism and environment. In: Jennings DH (ed) Integration of Activity in the Higher Plant. Cambridge University Press, Cambridge, pp 417-505

Cramer W, Kicklighter DW, Bondeau A, Moore III B, Churkina G, Nemry B, Ruimy A, Schloss AL, the Participants of the Potsdam NPP Model Intercomparison (1999) Comparing global models of terrestrial net primary productivity (NPP): overview and key results. Global Change Biol 5: 1-15. https://doi.org/10.1046/j.1365-2486.1999.00009.x

Cramer W, Bondeau A, Woodward FI, Prentice IC, Betts RA, Brovkin V, Cox PM, Fisher V, Foley JA, Friend AD (2001) Global response of terrestrial ecosystem structure and function to CO_2 and climate change: results from six dynamic global vegetation models. Global Change Biol 7: 357-373. https://doi.org/10.1046/j.1365-2486.2001.00383.x

Cuny HE, Rathgeber CBK, Kiessé TS, Hartmann FP, Barbeito I, Fournier M (2013) Generalized additive models reveal the intrinsic complexity of wood formation dynamics. J Exp Bot 64: 1983-1994. https://doi.org/10.1093/jxb/ert057

D'Andrea E, Scartazza A, Battistelli A, Collalti A, Proietti S, Rezaie N, Matteucci G, Moscatello S (2021) Unravelling resilience mechanisms in forests: role of non-structural carbohydrates in responding to extreme weather events. Tree Physiol 41: 1808-1818. https://doi.org/10.1093/treephys/tpab044

De Schepper V, Steppe K (2010) Development and verification of a water and sugar transport model using measured stem diameter variations. J Exp Bot 61: 2083-2099. https://doi.org/10.1093/jxb/erq018

De Schepper V, De Swaef T, Bauweraerts I, Steppe K (2013) Phloem transport: a review of mechanisms and controls. J Exp Bot 64: 4839-4850. https://doi.org/10.1093/jxb/ert302

Delpierre N, Vitasse Y, Chuine I, Guillemot J, Bazot S, Rutishauser T, Rathgeber CBK (2016a) Temperate and boreal forest tree phenology: from organ-scale processes to terrestrial ecosystem models. Ann For Sci 73: 5-25. https://doi.org/10.1007/s13595-015-0477-6

Delpierre N, Berveiller D, Granda E, Dufrêne E (2016b) Wood phenology, not carbon input, controls the interannual variability of wood growth in a temperate oak forest. New Phytol 210: 459-470. https://doi.org/10.1111/nph.13771

Deslauriers A, Rossi S, Anfodillo T (2007) Dendrometer and intra-annual tree growth: what kind of information can be inferred? Dendrochronologia 25: 113-124. https://doi.org/10.1016/j.dendro.2007.05.003

Dewar R (1995) Interpretation of an empirical model for stomatal conductance in terms of guard cell function. Plant Cell Environ 18: 365-372. https://doi.org/10.1111/j.1365-3040.1995.tb00372.x

Dewar R, Mauranen A, Mäkelä A, Hölttä T, Medlyn B, Vesala T (2018) New insights into the covariation of stomatal, mesophyll and hydraulic conductances from optimization models incorporating nonstomatal limitations to photosynthesis. New Phytol 217: 571-585. https://doi.org/10.1111/nph.14848

Dewar RC (2002) The Ball-Berry-Leuning and Tardieu-Davies stomatal models: synthesis and extension within a spatially aggregated picture of guard cell function. Plant Cell Environ 25: 1383-1398. https://doi.org/10.1046/j.1365-3040.2002.00909.x

Dietze MC (2017) Ecological Forecasting. Princeton University Press, Princeton

Domec J-Ch, King JS, Carmichael MJ, Overby AT, Wortemann R, Smith WK, Miao G, Noormets A, Johnson DM (2021) Aquaporins, and not changes in root structure, provide new insights into physiological responses to drought, flooding, and salinity. J Exp Bot 72: 4489-4501.

https://doi.org/10.1093/jxb/erab100

Duursma RA, Mäkelä A (2007) Summary models for light interception and light-use efficiency of non-homogeneous canopies. Tree Physiol 27: 859-870. https://doi.org/10.1093/treephys/27.6.859

Duursma RA, Kolari P, Perämäki M, Nikinmaa E, Hari P, Delzon S, Loustau D, Ilvesniemi H, Pumpanen J, Mäkelä A (2008) Predicting the decline in daily maximum transpiration rate of two pine stands during drought based on constant minimum leaf water potential and plant hydraulic conductance. Tree Physiol 28: 265-276. https://doi.org/10.1093/treephys/28.2.265

Duursma RA, Blackman ChJ, Lopéz R, Martin-StPaul NK, Cochard H, Medlyn BE (2019) On the minimum leaf conductance: its role in models of plant water use, and ecological and environmental controls. New Phytol 221: 693-705. https://doi.org/10.1111/nph.15395

Eckes-Shephard AH, Ljungqvist FCh, Drew DM, Rathgeber CBK, Friend AD (2022) Wood formation modelling – a research review and future perspectives. Front Plant Sci 13: article id 837648. https://doi.org/10.3389/fpls.2022.837648

Eitel JU, Griffin KL, Boelman NT, Maguire AJ, Meddens AJ, Jensen J, Vierling LA, Schmiege SC, Jennewein JS (2020) Remote sensing tracks daily radial wood growth of evergreen needleleaf trees. Global Change Biol 26: 4068-4078. https://doi.org/10.1111/gcb.15112

FAO (2020) The State of Food and Agriculture 2020. Overcoming water challenges in agriculture. Rome, Italy. https://doi.org/10.4060/cb1447en

Fatichi S, Pappas C, Zscheischler J, Leuzinger S (2019) Modelling carbon sources and sinks in terrestrial vegetation. New Phytol 221: 652-668. https://doi.org/10.1111/nph.15451

Friedlingstein P, Meinshausen M, Arora VK, Jones ChD, Anav A, Liddicoat SK, Knutti R (2014) Uncertainties in CMIP5 climate projections due to carbon cycle feedbacks. J Clim 27: 511-526. https://doi.org/10.1175/JCLI-D-12-00579.1

Friend AD, Eckes-Shephard AH, Fonti P, Rademacher TT, Rathgeber CBK, Richardson AD, Turton RH (2019) On the need to consider wood formation processes in global vegetation models and a suggested approach. Ann For Sci 76: 1-13. https://doi.org/10.1007/s13595-019-0819-x

Friend AD, Eckes-Shephard AH, Tupker Q (2022) Wood structure explained by complex spatial source-sink interactions. Nat Commun 13: article id 7824. https://doi.org/10.1038/s41467-022-35451-7

Galmés J, Hermida-Carrera C, Laanisto L, Niinemets Ü (2016) A compendium of temperature responses of Rubisco kinetic traits: variability among and within photosynthetic groups and impacts on photosynthesis modeling. J Exp Bot 67: 5067-5091. https://doi.org/10.1093/jxb/erw267

Gelman A, Carlin JB, Stern HS, Dunson DB, Vehtari A, Rubin DB (2014) Bayesian Data Analysis 3rd edition. CRC Press, Boca Raton. https://doi.org/10.1201/b16018

Gimeno TE, Stangl ZR, Barbeta A, Saavedra N, Wingate L, Devert N, Marshall JD (2022) Water taken up through the bark is detected in the transpiration stream in intact upper-canopy branches. Plant Cell Environ 45: 3219-3232. https://doi.org/10.1111/pce.14415

Gompertz B (1825) On the nature of the function expressive of the law of human mortality, and on a new mode of determining the value of life contingencies. Philos T R Soc Lond: 513-583. https://doi.org/10.1098/rstl.1825.0026

Gould N, Thorpe MR, Koroleva O, Minchin PE (2005) Phloem hydrostatic pressure relates to solute loading rate: a direct test of the Münch hypothesis. Funct Plant Biol 32: 1019-1026. https://doi.org/10.1071/FP05036

Granier A (1987) Evaluation of transpiration in a Douglas-fir stand by means of sap flow measurements. Tree Physiol 3: 309-320. https://doi.org/10.1093/treephys/3.4.309

Güney A, Zweifel R, Türkan S, Zimmermann R, Wachendorf M, Güney CO (2020) Drought responses and their effects on radial stem growth of two co-occurring conifer species in the Mediterranean mountain range. Ann For Sci 77: 1-16. https://doi.org/10.1007/s13595-020-01007-2

Hallema DW, Périard Y, Lafond JA, Gumiere SJ, Caron J (2015) Characterization of water retention curves for a series of cultivated Histosols. Vadose Zone J 14: 1-8. https://doi.org/10.2136/vzj2014.10.0148

Hari P, Kulmala M (2005) Station for measuring ecosystem-atmospheric relations (SMEAR II). Boreal Environ Res 10: 315-322

Hari P, Mäkelä A (2003) Annual pattern of photosynthesis in Scots pine in the boreal zone. Tree Physiol 23: 145-155. https://doi.org/10.1093/treephys/23.3.145

Hari P, Mäkelä A, Korpilahti E, Holmberg M (1986) Optimal control of gas exchange. Tree Physiol 2: 169-175. https://doi.org/10.1093/treephys/2.1-2-3.169

Härkönen S, Pulkkinen M, Duursma R, Mäkelä A (2010) Estimating annual GPP, NPP and stem growth in Finland using summary models. Forest Ecol Manag 259: 524-533. https://doi.org/10.1016/j.foreco.2009.11.009

Hartig F, Minunno F, Paul S (2019) BayesianTools: General-Purpose MCMC and SMC Samplers and Tools for Bayesian Statistics (R package version 0.1.6). https://CRANR-project.org/package=BayesianTools. Accessed via R v.4.3.1 9 January 2024.

Hartmann H, Trumbore S (2016) Understanding the roles of nonstructural carbohydrates in forest trees – from what we can measure to what we want to know. New Phytol 211: 386-403. https://doi.org/10.1111/nph.13955

Hartmann FP, Rathgeber CBK, Badel É, Fournier M, Moulia B (2021) Modelling the spatial crosstalk between two biochemical signals explains wood formation dynamics and tree-ring structure. J Exp Bot 72: 1727-1737. https://doi.org/10.1093/jxb/eraa558

Haverd V, Smith B, Nieradzik L, Briggs PR, Woodgate W, Trudinger CM, Canadell JG, Cuntz M (2018) A new version of the CABLE land surface model (Subversion revision r4601) incorporating land use and land cover change, woody vegetation demography, and a novel optimisation-based approach to plant coordination of photosynthesis. Geosci Model Dev 11: 2995-3026. https://doi.org/10.5194/gmd-11-2995-2018

Hayat A, Hacket-Pain AJ, Pretzsch H, Rademacher TT, Friend AD (2017) Modeling tree growth taking into account carbon source and sink limitations. Front Plant Sci 8, article id 182. https://doi.org/10.3389/fpls.2017.00182

Heinsoo K, Koppel A (1999) Minimum epidermal conductance of Norway spruce (Picea abies) needles: influence of age and shoot position in the crown. Ann Bot Fenn 35: 257-262

Helmisaari H-S, Derome J, Nöjd P, Kukkola M (2007) Fine root biomass in relation to site and stand characteristics in Norway spruce and Scots pine stands. Tree Physiol 27: 1493-1504. https://doi.org/10.1093/treephys/27.10.1493

Hökkä H, Laurén A, Stenberg L, Launiainen S, Leppä K, Nieminen M (2021) Defining guidelines for ditch depth in drained Scots pine dominated peatland forests. Silva Fenn 55, article id 10494. https://doi.org/10.14214/sf.10494

Hölttä T, Mäkinen H, Nöjd P, Mäkelä A, Nikinmaa E (2010) A physiological model of softwood cambial growth. Tree Physiol 30: 1235-1252. https://doi.org/10.1093/treephys/tpq068

Hölttä T, Linkosalo T, Riikonen A, Sevanto S, Nikinmaa E (2015) An analysis of Granier sap flow method, its sensitivity to heat storage and a new approach to improve its time dynamics. Agr Forest Meteorol 211: 2-12. https://doi.org/10.1016/j.agrformet.2015.05.005

Hölttä T, Lintunen A, Chan T, Mäkelä A, Nikinmaa E (2017) A steady-state stomatal model of balanced leaf gas exchange, hydraulics and maximal source-sink flux. Tree Physiol 37: 851-868. https://doi.org/10.1093/treephys/tpx011

Huang J-B, Hammerbacher A, Gershenzon J, Van Dam NM, Sala A, McDowell NG, Chowdhury S, Gleixner G, Trumbore S, Hartmann H (2021) Storage of carbon reserves in spruce trees is prioritized over growth in the face of carbon limitation. P Natl Acad Sci USA 118, article id e2023297118. https://doi.org/10.1073/pnas.2023297118

IPCC (2023) Summary for policymakers. In: Core Writing Team, Lee H, Romero J (eds.) Climate Change 2023: Synthesis Report, Contribution of Working Groups I, II and III to the Sixth Assessment Report of the Intergovernmental Panel on Climate Change. IPCC, Geneva

Jager MM, Richardson SJ, Bellingham PJ, Clearwater MJ, Laughlin DC (2015) Soil fertility

induces coordinated responses of multiple independent functional traits. J Ecol 103: 374-385. https://doi.org/10.1111/1365-2745.12366

Jarvis P (1976) The interpretation of the variations in leaf water potential and stomatal conductance found in canopies in the field. Philos T Roy Soc B 273: 593-610. https://doi.org/10.1098/rstb.1976.0035

Jarvis PG, McNaughton KG (1986) Stomatal control of transpiration: scaling up from leaf to region. Adv Ecol Res 15: 1-49. https://doi.org/10.1016/S0065-2504(08)60119-1

Johnson FH, Eyring H, Williams R (1942) The nature of enzyme inhibitions in bacterial luminescence: sulfanilamide, urethane, temperature and pressure. J Cell Compar Physl 20: 247-268. https://doi.org/10.1002/jcp.1030200302

Jones HG (2014) Plants and Microclimate: A Quantitative Approach to Environmental Plant Physiology 3rd edition. Cambridge University Press, New York. https://doi.org/10.1017/CBO9780511845727

Jyske T, Mäkinen H, Kalliokoski T, Nöjd P (2014) Intra-annual tracheid production of Norway spruce and Scots pine across a latitudinal gradient in Finland. Agr Forest Meteorol 194: 241-254. https://doi.org/10.1016/j.agrformet.2014.04.015

Kacser H, Fell D (1995) The control of flux. Biochem Soc T 23: 341-366. https://doi.org/10.1042/bst0230341

Kellomäki S, Wang K-Y (1996) Photosynthetic responses to needle water potentials in Scots pine after a four-year exposure to elevated CO_2 and temperature. Tree Physiol 16: 765-772. https://doi.org/10.1093/treephys/16.9.765

Knauer J, Zaehle S, Medlyn BE, Reichstein M, Williams ChA, Migliavacca M, De Kauwe MG, Werner Ch, Keitel C, Kolari P, Limousin J-M, Linderson M-L (2018) Towards physiologically meaningful water-use efficiency estimates from eddy covariance data. Glob Change Biol 24: 694-710. https://doi.org/10.1111/gcb.13893

Knoblauch M, Knoblauch J, Mullendore DL, Savage JA, Babst BA, Beecher SD, Dodgen AC, Jensen KH, Holbrook NM (2016) Testing the Münch hypothesis of long distance phloem transport in plants. Elife 5: e15341. https://doi.org/10.7554/eLife.15341

Koch GW, Sillett SC, Jennings GM, Davis SD (2004) The limits to tree height. Nature 428: 851-854. https://doi.org/10.1038/nature02417

Kolari P, Lappalainen HK, Hänninen H, Hari P (2007) Relationship between temperature and the seasonal course of photosynthesis in Scots pine at northern timberline and in southern boreal zone. Tellus B 59: 542-552. https://doi.org/10.1111/j.1600-0889.2007.00262.x

Kolari P, Chan T, Porcar-Castell A, Bäck J, Nikinmaa E, Juurola E (2014) Field and controlled environment measurements show strong seasonal acclimation in photosynthesis and respiration

potential in boreal Scots pine. Front Plant Sci 5: 717. https://doi.org/10.3389/fpls.2014.00717

Körner Ch (2015) Paradigm shift in plant growth control. Curr Opin Plant Biol 25: 107-114. https://doi.org/10.1016/j.pbi.2015.05.003

Kramer-Walter KR, Bellingham PJ, Millar TR, Smissen RD, Richardson SJ, Laughlin DC (2016) Root traits are multidimensional: specific root length is independent from root tissue density and the plant economic spectrum. J Ecol 104: 1299-1310. https://doi.org/10.1111/1365-2745.12562

Kruschke J (2014) Doing Bayesian Data Analysis: A Tutorial with R, JAGS, and Stan 2nd edition. Academic Press, San Diego. https://doi.org/10.1016/B978-0-12-405888-0.00008-8

Lambers H, Chapins III FS, Pons ThL (2014) Plant Physiological Ecology 2nd edition. Springer, New York

Laurila T, Aurela M, Hatakka J, Hotanen J-P, Jauhiainen J, Korkiakoski M, Korpela L, Koskinen M, Laiho R, Lehtonen A, Leppä K, Linkosalmi M, Lohila A, Minkkinen K, Mäkelä T, Mäkiranta P, Nieminen M, Ojanen P, Peltoniemi M, Penttilä T, Rainne J, Rautakoski H, Saarinen M, Salovaara P, Sarkkola S, Mäkipää R (2021) Set-up and instrumentation of the greenhouse gas (GHG) measurements on experimental sites of continuous cover forestry. In: Natural Resources and Bioeconomy Studies 06/2021. Natural Resources Institute Finland (Luke), Helsinki. ISBN 978-952-380-191-2 (online).

Lehto J (1964) Käytännön metsätyypit [Forest types in practice]. Kirjayhtymä, Helsinki. ISBN 951-26-3101-6 nidottu [paperback].

Leppä K, Hökkä H, Laiho R, Launiainen S, Lehtonen A, Mäkipää R, Peltoniemi M, Saarinen M, Sarkkola S, Nieminen M (2020) Selection cuttings as a tool to control water table level in boreal drained peatland forests. Front Earth Sci 8, article id 428. https://doi.org/10.3389/feart.2020.576510

Leuning R (1995) A critical appraisal of a combined stomatal-photosynthesis model for C3 plants. Plant Cell Environ 18: 339-355. https://doi.org/10.1111/j.1365-3040.1995.tb00370.x

Leuschner Ch, Hertel D, Schmid I, Koch O, Muhs A, Hölscher D (2004) Stand fine root biomass and fine root morphology in old-growth beech forests as a function of precipitation and soil fertility. Plant Soil 258: 43-56. https://doi.org/10.1023/B:PLSO.0000016508.20173.80

Lin Y-S, Medlyn BE, Duursma RA, Prentice IC, Wang H, Baig S, Eamus D, De Dios VR, Mitchell P, Ellsworth DS (2015) Optimal stomatal behaviour around the world. Nat Clim Change 5: 459-464. https://doi.org/10.1038/nclimate2550

Linkosalo T, Häkkinen R, Hänninen H (2006) Models of the spring phenology of boreal and temperate trees: Is there something missing? Tree Physiol 26: 1165-1172. https://doi.org/10.1093/treephys/26.9.1165

Lockhart JA (1965) An analysis of irreversible plant cell elongation. J Theor Biol 8: 264-275. https://doi.org/10.1016/0022-5193(65)90077-9

Lu P, Urban L, Zhao P (2004) Granier's thermal dissipation probe (TDP) method for measuring sap flow in trees: theory and practice. Acta Bot Sin 46: 631-646

Lu Y-J, Duursma RA, Farrior CE, Medlyn BE, Feng X (2020) Optimal stomatal drought response shaped by competition for water and hydraulic risk can explain plant trait covariation. New Phytol 225: 1206-1217. https://doi.org/10.1111/nph.16207

Mäkelä A (1997) A carbon balance model of growth and self-pruning in trees based on structural relationships. Forest Sci 43: 7-24. https://doi.org/10.1093/forestscience/43.1.7

Mäkelä A, Valentine HT (2020) Models of Tree and Stand Dynamics. Springer, Cham. https://doi.org/10.1007/978-3-030-35761-0

Mäkelä A, Hari P, Berninger F, Hänninen H, Nikinmaa E (2004) Acclimation of photosynthetic capacity in Scots pine to the annual cycle of temperature. Tree Physiol 24: 369-376. https://doi.org/10.1093/treephys/24.4.369

Mäkelä A, Pulkkinen M, Kolari P, Lagergren F, Berbigier P, Lindroth A, Loustau D, Nikinmaa E, Vesala T, Hari P (2008) Developing an empirical model of stand GPP with the LUE approach: analysis of eddy covariance data at five contrasting conifer sites in Europe. Global Change Biol 14: 92-108. https://doi.org/10.1111/j.1365-2486.2007.01463.x

Mäkelä A, Tian X-L, Repo A, Ilvesniemi H, Marshall J, Minunno F, Näsholm T, Schiestl-Aalto P, Lehtonen A (2022) Do mycorrhizal symbionts drive latitudinal trends in photosynthetic carbon use efficiency and carbon sequestration in boreal forests? Forest Ecol Manag 520, article id 120355. https://doi.org/10.1016/j.foreco.2022.120355

Mäkinen H, Nöjd P, Saranpää P (2003) Seasonal changes in stem radius and production of new tracheids in Norway spruce. Tree Physiol 23: 959-968. https://doi.org/10.1093/treephys/23.14.959

Manzoni S, Vico G, Katul G, Palmroth S, Jackson RB, Porporato A (2013) Hydraulic limits on maximum plant transpiration and the emergence of the safety–efficiency trade-off. New Phytol 198: 169-178. https://doi.org/10.1111/nph.12126

Markkanen T, Rannik Ü, Keronen P, Suni T, Vesala T (2001) Eddy covariance fluxes over a boreal Scots pine forest. Boreal Environ Res 6: 65-78

Martínez-Vilalta J, Cochard H, Mencuccini M, Sterck F, Herrero A, Korhonen J, Llorens P, Nikinmaa E, Nole A, Poyatos R (2009) Hydraulic adjustment of Scots pine across Europe. New Phytol 184: 353-364. https://doi.org/10.1111/j.1469-8137.2009.02954.x

McDowell N, Barnard H, Bond B, Hinckley T, Hubbard R, Ishii H, Köstner B, Magnani F, Marshall J, Meinzer F (2002) The relationship between tree height and leaf area: sapwood area

ratio. Oecologia 132: 12-20. https://doi.org/10.1007/s00442-002-0904-x

McDowell NG, Bond BJ, Dickman LT, Ryan MG, Whitehead D (2011) Relationships between tree height and carbon isotope discrimination. In: Meinzer FC, Lachenbruch B, Dawson TE (eds) Size- and Age-Related Changes in Tree Structure and Function. Springer, Dordrecht, pp 255-286. https://doi.org/10.1007/978-94-007-1242-3_10

McMurtrie R, Wolf L (1983) Above-and below-ground growth of forest stands: a carbon budget model. Ann Bot-London 52: 437-448. https://doi.org/10.1093/oxfordjournals.aob.a086599

Medlyn BE, Duursma RA, Eamus D, Ellsworth DS, Prentice IC, Barton CV, Crous KY, De Angelis P, Freeman M, Wingate L (2011) Reconciling the optimal and empirical approaches to modelling stomatal conductance. Global Change Biol 17: 2134-2144. https://doi.org/10.1111/j.1365-2486.2010.02375.x

Medlyn BE, Duursma RA, Eamus D, Ellsworth DS, Colin Prentice I, Barton CV, Crous KY, Angelis P, Freeman M, Wingate L (2012) Reconciling the optimal and empirical approaches to modelling stomatal conductance. Global Change Biol 18, article id 3476. https://doi.org/10.1111/j.1365-2486.2012.02790.x

Mencuccini M, Hölttä T, Sevanto S, Nikinmaa E (2013) Concurrent measurements of change in the bark and xylem diameters of trees reveal a phloem-generated turgor signal. New Phytol 198: 1143-1154. https://doi.org/10.1111/nph.12224

Mencuccini M, Salmon Y, Mitchell P, Hölttä T, Choat B, Meir P, O'grady A, Tissue D, Zweifel R, Sevanto S (2017) An empirical method that separates irreversible stem radial growth from bark water content changes in trees: theory and case studies. Plant Cell Environ 40: 290-303. https://doi.org/10.1111/pce.12863

Metropolis N, Ulam S (1949) The Monte Carlo method. J Am Stat Assoc 44: 335-341. https://doi.org/10.1080/01621459.1949.10483310

Metropolis N, Rosenbluth AW, Rosenbluth MN, Teller AH, Teller E (1953) Equation of state calculations by fast computing machines. J Chem Phys 21: 1087-1092. https://doi.org/10.1063/1.1699114

Millard P, Sommerkorn M, Grelet G-A (2007) Environmental change and carbon limitation in trees: a biochemical, ecophysiological and ecosystem appraisal. New Phytol 175: 11-28. https://doi.org/10.1111/j.1469-8137.2007.02079.x

Moldrup P, Kruse C, Rolston D, Yamaguchi T (1996) Modeling diffusion and reaction in soils: III. Predicting gas diffusivity from the Campbell soil-water retention model. Soil Sci 161: 366-375. https://doi.org/10.1097/00010694-199606000-00003

Moldrup P, Olesen T, Rolston D, Yamaguchi T (1997) Modeling diffusion and reaction in soils: VII. Predicting gas and ion diffusivity in undisturbed and sieved soils. Soil Sci 162: 632-640. https://doi.org/10.1097/00010694-199709000-00004

Münch E (1930) Die Stoffbewegungen in der Pflanze [The substance movements in the plant]. Gustav Fischer, Jena.

Newman E (1969) Resistance to water flow in soil and plant. I. Soil resistance in relation to amounts of root: theoretical estimates. J Appl Ecol: 1-12. https://doi.org/10.2307/2401297

Newton I (1959) Newton to Hooke, 5 February 1675/6. In: Turnbull HW (ed) The Correspondence of Isaac Newton, vol I. Cambridge University Press for the Royal Society, London

Niinemets Ü (2002) Stomatal conductance alone does not explain the decline in foliar photosynthetic rates with increasing tree age and size in Picea abies and Pinus sylvestris. Tree Physiol 22: 515-535. https://doi.org/10.1093/treephys/22.8.515

Nikinmaa E, Hölttä T, Hari P, Kolari P, Mäkelä A, Sevanto S, Vesala T (2013) Assimilate transport in phloem sets conditions for leaf gas exchange. Plant Cell Environ 36: 655-669. https://doi.org/10.1111/pce.12004

Nikinmaa E, Sievänen R, Hölttä T (2014) Dynamics of leaf gas exchange, xylem and phloem transport, water potential and carbohydrate concentration in a realistic 3-D model tree crown. Ann Bot-London 114: 653-666. https://doi.org/10.1093/aob/mcu068

Nobel PS (2020) Physicochemical and Environmental Plant Physiology 5th edition. Academic Press, San Diego

Ogata K (2010) Modern Control Engineering 5th edition. Prentice Hall, Upper Saddle River

Oishi ACh, Oren R, Stoy PC (2008) Estimating components of forest evapotranspiration: a footprint approach for scaling sap flux measurements. Agr Forest Meteorol 148: 1719-1732. https://doi.org/10.1016/j.agrformet.2008.06.013

Oishi ACh, Hawthorne DA, Oren R (2016) Baseliner: an open-source, interactive tool for processing sap flux data from thermal dissipation probes. SoftwareX 5: 139-143. https://doi.org/10.1016/j.softx.2016.07.003

Ostonen I, Lõhmus K, Helmisaari H-S, Truu J, Meel S (2007) Fine root morphological adaptations in Scots pine, Norway spruce and silver birch along a latitudinal gradient in boreal forests. Tree Physiol 27: 1627-1634. https://doi.org/10.1093/treephys/27.11.1627

Päivänen J (1973) Hydraulic conductivity and water retention in peat soils. Acta For Fenn 129. https://doi.org/10.14214/aff.7563

Paljakka T, Jyske T, Lintunen A, Aaltonen H, Nikinmaa E, Hölttä T (2017) Gradients and dynamics of inner bark and needle osmotic potentials in Scots pine (*Pinus sylvestris* L.) and Norway spruce (*Picea abies* (L.) Karst). Plant Cell Environ 40: 2160-2173. https://doi.org/10.1111/pce.13017

Parent B, Tardieu F (2012) Temperature responses of developmental processes have not been affected by breeding in different ecological areas for 17 crop species. New Phytol 194: 760-774. https://doi.org/10.1111/j.1469-8137.2012.04086.x

Parent B, Turc O, Gibon Y, Stitt M, Tardieu F (2010) Modelling temperature-compensated physiological rates, based on the co-ordination of responses to temperature of developmental processes. J Exp Bot 61: 2057-2069. https://doi.org/10.1093/jxb/erq003

Peltoniemi M, Pulkkinen M, Aurela M, Pumpanen J, Kolari P, Mäkelä A (2015) A semi-empirical model of boreal-forest gross primary production, evapotranspiration, and soil water — calibration and sensitivity analysis. Boreal Environ Res 20: 151-171

Penman HL (1940) Gas and vapor movements in soil: The diffusion of vapors through porous solids. J Agr Sci 30: 437-462. https://doi.org/10.1017/S0021859600048164

Perez-Priego O, Katul G, Reichstein M, El-Madany TS, Ahrens B, Carrara A, Scanlon TM, Migliavacca M (2018) Partitioning eddy covariance water flux components using physiological and micrometeorological approaches. J Geophys Res-Biogeo 123: 3353-3370. https://doi.org/10.1029/2018JG004637

Perri S, Katul GG, Molini A (2019) Xylem-phloem hydraulic coupling explains multiple osmoregulatory responses to salt stress. New Phytol 224: 644-662. https://doi.org/10.1111/nph.16072

Phillips N, Nagchaudhuri A, Oren R, Katul G (1997) Time constant for water transport in loblolly pine trees estimated from time series of evaporative demand and stem sapflow. Trees 11: 412-419. https://doi.org/10.1007/s004680050102

Phillips NG, Oren R, Licata J, Linder S (2004) Time series diagnosis of tree hydraulic characteristics. Tree Physiol 24: 879-890. https://doi.org/10.1093/treephys/24.8.879

Potkay A, Trugman AT, Wang Y-J, Venturas MD, Anderegg WR, Mattos CR, Fan Y (2021) Coupled whole-tree optimality and xylem hydraulics explain dynamic biomass partitioning. New Phytol 230: 2226-2245. https://doi.org/10.1111/nph.17242

Poyatos R, Aguadé D, Martínez-Vilalta J (2018) Below-ground hydraulic constraints during drought-induced decline in Scots pine. Ann For Sci 75: 1-14. https://doi.org/10.1007/s13595-018-0778-7

R Development Core Team (2019, 2020, 2022) R: a language and environment for statistical computing, v.3.5.3, v.4.0.3, v.4.2.1. R foundation for Statistical Computing, Vienna. http://www.r-project.org. Accessed 9 January 2024.

Repola J (2009) Biomass equations for Scots pine and Norway spruce in Finland. Silva Fenn 43: 625-647. https://doi.org/10.14214/sf.184

Ryan MG, Phillips N, Bond BJ (2006) The hydraulic limitation hypothesis revisited. Plant Cell

Environ 29: 367-381. https://doi.org/10.1111/j.1365-3040.2005.01478.x

Schäfer C, Rötzer T, Thurm EA, Biber P, Kallenbach C, Pretzsch H (2019) Growth and tree water deficit of mixed Norway spruce and European beech at different heights in a tree and under heavy drought. Forests 10, article id 577. https://doi.org/10.3390/f10070577

Schiestl-Aalto P, Kulmala L, Mäkinen H, Nikinmaa E, Mäkelä A (2015) CASSIA – a dynamic model for predicting intra-annual sink demand and interannual growth variation in Scots pine. New Phytol 206: 647-659. https://doi.org/10.1111/nph.13275

Schiestl-Aalto P, Stangl ZR, Tarvainen L, Wallin G, Marshall J, Mäkelä A (2021) Linking canopy-scale mesophyll conductance and phloem sugar δ13C using empirical and modelling approaches. New Phytol 229: 3141-3155. https://doi.org/10.1111/nph.17094

Scholz FG, Phillips NG, Bucci SJ, Meinzer FC, Goldstein G (2011) Hydraulic capacitance: biophysics and functional significance of internal water sources in relation to tree size. In: Meinzer FC, Lachenbruch B, Dawson TE (eds) Size- and Age-Related Changes in Tree Structure and Function. Springer, Dordrecht, pp 341-361. https://doi.org/10.1007/978-94-007-1242-3_13

Sellers P, Mintz Y, Sud YC, Dalcher A (1986) A simple biosphere model (SiB) for use within general circulation models. J Atmos Sci 43: 505-531. https://doi.org/10.1175/1520-0469(1986)043%3C0505:ASBMFU%3E2.0.CO;2

Sevanto S, Hölttä T, Hirsikko A, Vesala T, Nikinmaa E (2005) Determination of thermal expansion of green wood and the accuracy of tree stem diameter variation measurements. Boreal Environ Res 10: 437

Sivia D, Skilling J (2006) Data Analysis: A Bayesian Tutorial 2nd edition. Oxford University Press, Oxford. https://doi.org/10.1093/oso/9780198568315.001.0001

Sorce C, Giovannelli A, Sebastiani L, Anfodillo T (2013) Hormonal signals involved in the regulation of cambial activity, xylogenesis and vessel patterning in trees. Plant Cell Rep 32: 885-898. https://doi.org/10.1007/s00299-013-1431-4

Sperry JS, Venturas MD, Anderegg WR, Mencuccini M, Mackay DS, Wang Y-J, Love DM (2017) Predicting stomatal responses to the environment from the optimization of photosynthetic gain and hydraulic cost. Plant Cell Environ 40: 816-830. https://doi.org/10.1111/pce.12852

Stenberg L, Haahti K, Hökkä H, Launiainen S, Nieminen M, Laurén A, Koivusalo H (2018) Hydrology of drained peatland forest: Numerical experiment on the role of tree stand heterogeneity and management. Forests 9, article id 645. https://doi.org/10.3390/f9100645

Steppe K, De Pauw DJ, Lemeur R, Vanrolleghem PA (2006) A mathematical model linking tree sap flow dynamics to daily stem diameter fluctuations and radial stem growth. Tree Physiol 26: 257-273. https://doi.org/10.1093/treephys/26.3.257

Steppe K, De Pauw DJ, Doody TM, Teskey RO (2010) A comparison of sap flux density using thermal dissipation, heat pulse velocity and heat field deformation methods. Agr Forest Meteorol 150: 1046-1056. https://doi.org/10.1016/j.agrformet.2010.04.004

Steppe K, Niinemets Ü, Teskey RO (2011) Tree size- and age-related changes in leaf physiology and their influence on carbon gain. In: Meinzer FC, Lachenbruch B, Dawson TE (eds) Size- and Age-Related Changes in Tree Structure and Function. Springer, Dordrecht, pp 235-254. https://doi.org/10.1007/978-94-007-1242-3_9

Tardieu F, Davies W (1993) Integration of hydraulic and chemical signalling in the control of stomatal conductance and water status of droughted plants. Plant Cell Environ 16: 341-349. https://doi.org/10.1111/j.1365-3040.1993.tb00880.x

Taylor CJ, Pedregal DJ, Young PC, Tych W (2007) Environmental time series analysis and forecasting with the Captain toolbox. Environ Modell Softw 22: 797-814. https://doi.org/10.1016/j.envsoft.2006.03.002

Thornley JH, Johnson IR (1990) Plant and crop modelling. Clarendon Press, Oxford

Tian X-L, Minunno F, Cao T-J, Peltoniemi M, Kalliokoski T, Mäkelä A (2020) Extending the range of applicability of the semi-empirical ecosystem flux model PRELES for varying forest types and climate. Global Change Biol 26: 2923-2943. https://doi.org/10.1111/gcb.14992

Tor-Ngern P, Oren R, Oishi ACh, Uebelherr JM, Palmroth S, Tarvainen L, Ottosson-Löfvenius M, Linder S, Domec J-Ch, Näsholm T (2017) Ecophysiological variation of transpiration of pine forests: synthesis of new and published results. Ecol Appl 27: 118-133. https://doi.org/10.1002/eap.1423

Tyree MT, Yang Sh-D (1990) Water-storage capacity of Thuja, Tsuga and Acer stems measured by dehydration isotherms: the contribution of capillary water and cavitation. Planta 182: 420-426. https://doi.org/10.1007/BF02411394

Tyree MT, Zimmermann MH (2002) Xylem Structure and the Ascent of Sap 2nd edition. Springer-Verlag, Berlin Heidelberg. https://doi.org/10.1007/978-3-662-04931-0

Vaganov EA, Hughes MK, Shashkin AV (2006) Growth Dynamics of Conifer Tree Rings: Images of Past and Future Environments. Springer-Verlag, Heidelberg

Valentine HT, Herman DA, Gove JH, Hollinger DY, Solomon DS (2000) Initializing a model stand for process-based projection. Tree Physiol 20: 393-398. https://doi.org/10.1093/treephys/20.5-6.393

Van Genuchten MT (1980) A closed-form equation for predicting the hydraulic conductivity of unsaturated soils. Soil Sci Soc Am J 44: 892-898. https://doi.org/10.2136/sssaj1980.03615995004400050002x

Vanninen P, Mäkelä A (1999) Fine root biomass of Scots pine stands differing in age and soil

fertility in southern Finland. Tree Physiology 19: 823-830. https://doi.org/10.1093/treephys/19.12.823

Vanninen P, Ylitalo H, Sievänen R, Mäkelä A (1996) Effects of age and site quality on the distribution of biomass in Scots pine (*Pinus sylvestris* L.). Trees 10: 231-238. https://doi.org/10.1007/BF02185674

Vogt KA, Vogt DJ, Asbjornsen H, Dahlgren RA (1995) Roots, nutrients and their relationship to spatial patterns. Plant Soil 168: 113-123. https://doi.org/10.1007/BF00029320

Vrugt JA, Ter Braak CJ, Gupta HV, Robinson BA (2009) Equifinality of formal (DREAM) and informal (GLUE) Bayesian approaches in hydrologic modeling? Stoch Env Res Risk A 23: 1011-1026. https://doi.org/10.1007/s00477-008-0274-y

West GB, Brown JH, Enquist BJ (1999) A general model for the structure and allometry of plant vascular systems. Nature 400: 664-667. https://doi.org/10.1038/23251

Winsor CP (1932) The Gompertz curve as a growth curve. P Natl Acad Sci USA 18: 1-8. https://doi.org/10.1073/pnas.18.1.1

Wodzicki T (1971) Mechanism of xylem differentiation in *Pinus silvestris* L. J Exp Bot 22: 670-687. https://doi.org/10.1093/jxb/22.3.670

Wright AJ, de Kroon H, Visser EJ, Buchmann T, Ebeling A, Eisenhauer N, Fischer C, Hildebrandt A, Ravenek J, Roscher C (2017) Plants are less negatively affected by flooding when growing in species-rich plant communities. New Phytol 213: 645-656. https://doi.org/10.1111/nph.14185

Young PC (2000) Stochastic, dynamic modelling and signal processing: time variable and state dependent parameter estimation. In: Fitzgerald WJ, Smith RL, Walden AT, Young PC (eds) Nonlinear and Nonstationary Signal Processing. Cambridge University Press, Cambridge, pp 74-115

Young PC, McKenna P, Bruun J (2001) Identification of non-linear stochastic systems by state dependent parameter estimation. Int J Control 74: 1837-1857. https://doi.org/10.1080/00207170110089824

Zeide B (1993) Analysis of growth equations. For Sci 39: 594-616. https://doi.org/10.1093/forestscience/39.3.594

Zuidema PA, Poulter B, Frank DC (2018) A wood biology agenda to support global vegetation modelling. Trends Plant Sci 23: 1006-1015. https://doi.org/10.1016/j.tplants.2018.08.003

Zweifel R, Haeni M, Buchmann N, Eugster W (2016) Are trees able to grow in periods of stem shrinkage? New Phytol 211: 839-849. https://doi.org/10.1111/nph.13995

Zweifel R, Etzold S, Sterck F, Gessler A, Anfodillo T, Mencuccini M, von Arx G, Lazzarin M,

Haeni M, Feichtinger L (2020) Determinants of legacy effects in pine trees–implications from an irrigation-stop experiment. New Phytol 227: 1081-1096. https://doi.org/10.1111/nph.16582